Chemosphere 368 (2024) 143711

Contents lists available at ScienceDirect

Chemosphere

journal homepage: www.elsevier.com/locate/chemosphere

Uranium adsorption by iron modified zeolite and zeolite composite membranes

Akhil Gopalakrishnan, Stephen Asare, Francis Adu-Boahene, Andrea I. Schäfer *

Institute for Advanced Membrane Technology (IAMT), Karlsruhe Institute of Technology (KIT), Hermann-von-Helmholtz-Platz 1, 76344, Eggenstein-Leopoldshafen, Germany

HIGHLIGHTS

- High Si/Al ratio zeolites show the best uranium uptake in neutral to alkaline pH.
- Fe-zeolite uranium uptake in static adsorption is 60% lower than in filtration.
- Ionic strength above 2.5 g/L NaCl does not impact uranium uptake.
- PHREEQC modeling validates observed uranium adsorption mechanisms on zeolite.
- Uranium uptake in MF/UF membranes is flow rate - and time-dependent.

GRAPHICAL ABSTRACT

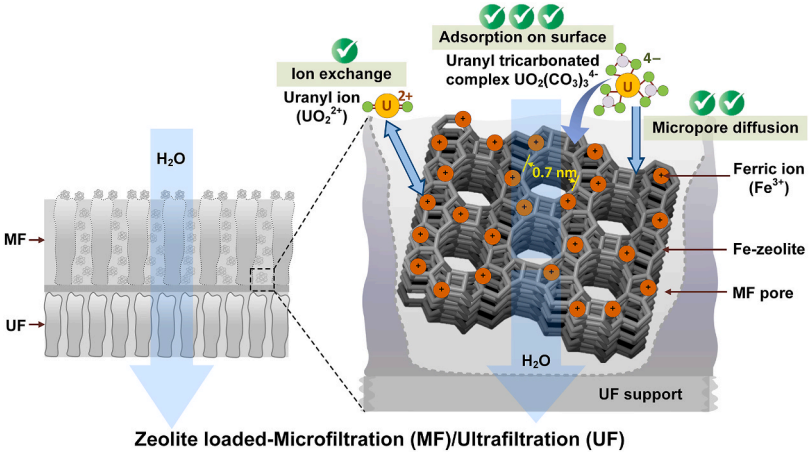

ARTICLE INFO

Handling editor: Y Yeomin Yoon

Keywords:
Physico-chemical water treatment
Heavy metal removal
Ultrafiltration
Aluminosilicates
Membrane technology
PHREEQC modeling

ABSTRACT

Composite membranes incorporated with high-performance adsorbents are promising for uranium removal. The impact of speciation and ionic strength on uranium adsorption by zeolites was investigated in both static adsorption and composite membrane filtration. Zeolites with high Si/Al ratios exhibited the highest uranium adsorption capacity. Iron-modified zeolite, BEA-Fe30 completely removed uranium at a concentration of 0.6 g/L in static adsorption, with uranium uptake ranging from 125 to 130 μg/g at pH values between 6 and 12. At lower pH values, uptake decreased, dropping to 3 μg/g at pH 2. The increased uranium uptake between pH 6 and 12 is attributed to the formation of a ternary complex involving U(VI), carbonate, and Fe oxide surface (hydr)oxo sites. High ionic strength did not impact the adsorption of uranium. Additionally, PHREEQC modeling was employed to simulate uranium speciation and adsorption behavior under varying pH and ionic strength conditions, further validating experimental findings. Zeolite-loaded microfiltration/ultrafiltration (MF/UF) membranes achieved the WHO guideline of 30 μg/L uranium in the permeate, using less zeolite compared to static adsorption. With 0.25 g of zeolite, the MF/UF process achieved a uranium uptake of 699 μg/g, significantly higher than the 256 μg/g observed in static adsorption. However, uranium removal decreased with increased flow rates, suggesting

* Corresponding author.
E-mail address: Andrea.Iris.Schaefer@kit.edu (A.I. Schäfer).

https://doi.org/10.1016/j.chemosphere.2024.143711
Received 17 July 2024; Received in revised form 5 November 2024; Accepted 6 November 2024
Available online 21 November 2024

mass transfer limitations during filtration. The study highlights the potential of composite membranes with high-performance zeolites for efficient uranium removal, contributing to advancements in water purification technologies and addressing environmental contamination.

1. Introduction

Uranium is a naturally occurring radioactive element in varied drinking water concentrations (Smedley and Kinniburgh, 2023; Abolli et al., 2024). Drinking water is estimated to account for 57–84% of the daily uranium intake in a typical human diet (Haneklaus et al., 2021). Despite reports of a low global average of uranium in fresh water, such as 0.3 μg/L for surface water (Mangini et al., 1979), there have been regular occurrences of uranium concentrations above the current WHO provisional guideline limit of 30 μg/L (WHO, 2017) in certain drinking waters (Smedley and Kinniburgh, 2023). The US Environmental Protection Agency (EPA) has set a regulatory standard of 30 μg/L, whereas some countries have recommended even more stringent guideline limits, for example Japan (2 μg/L) (MHLW, 2015), Germany (10 μg/L) (Bundesgesetzblatt, 2023), and Canada (20 μg/L) (Health Canada, 2019). The presence of uranium in drinking water poses considerable health hazards due to the chemical toxicity of uranium, which can result in chronic kidney disease (WHO, 2017).

Removing uranium from polluted water sources is crucial due to its radioactivity and chemical toxicity. Several methods, such as adsorption (Jiménez-Reyes et al., 2021; Jun et al., 2021; Ighalo et al., 2024; Mittal et al., 2024), ion exchange (Li et al., 2022a), co-precipitation (Luo et al., 2009), bioremediation (Ighalo et al., 2024), and membrane filtration (Raff and Wilken, 1999; Shen and Schäfer, 2014; Xing et al., 2023; Ighalo et al., 2024), can remove uranium from water based on the charge, affinity, and size of uranium species. Adsorption is the most researched technique, mainly using clay minerals (Akash et al., 2022; Gandhi et al., 2022), carbon-based adsorbents (Mittal et al., 2024), metal-organic frameworks (Rani et al., 2023), layered double hydroxides (He et al., 2023), and biosorbents (Akash et al., 2022). Among these, clay minerals (aluminosilicates) stand out due to their abundance, low cost, high ionic exchange capacity, water stability, and large surface area (Uddin, 2017).

Despite the high removal efficiency and relatively low costs of adsorption, certain challenges remain, such as limited capacity, non-selective adsorption, regeneration, and leaching of contaminants (Li et al., 2022a; Ighalo et al., 2024). Membrane filtration, which separates contaminants based on size or charge, offers a relatively small footprint and technical maturity (Qasem et al., 2021). Combining adsorption with membrane filtration may enhance selective separation and mitigate limitations like fouling, leaching, and kinetic issues (Davoodbeygi et al., 2023). However, hybrid processes may face challenges with uranium removal due to its complex chemical speciation, which affects interactions with solutes and surfaces. Uranium's speciation in water varies with pH, alkalinity, and complexing agents, influencing reactivity and treatment effectiveness. Therefore, understanding uranium speciation is key to assessing its solubility, toxicity, and removal efficiency (Smedley and Kinniburgh, 2023; Abolli et al., 2024).

The oxidation state of uranium is the key factor determining its environmental mobility. It is regulated by the pH, ionic strength, exchangeable cation composition, and dissolved CO_2 at varied temperatures and pressures (Maher et al., 2013; Nekhunguni et al., 2017). Uranium exists in various natural oxidation states such as +3, +4, +5, and +6, among which the tetravalent (U(IV)) and hexavalent (U(VI)) oxidation states predominate at common surface water and groundwater redox conditions (Maher et al., 2013; Gandhi et al., 2022). U(IV) forms immobile UO_2 near neutral pH due to low solubility, while U(VI) is soluble, mobile, and toxic as stable aqueous complexes of the uranyl ion UO_2^{2+} (Maher et al., 2013; Gandhi et al., 2022). The uranyl ion forms covalent bonds linearly with two oxygen atoms with an axial bond length of 1.77 Å (Kalintsev et al., 2023). At pH greater than 4, UO_2^{2+} forms polynuclear species like dimers (e.g., $(UO_2)_2(OH)_2^{2+}$) and trimers (e.g., $(UO_2)_3(OH)_5^{+}$) due to hydrolysis (Choppin and Jensen, 2006). It also forms complexes with ligands such as carbonate, phosphate, and sulfate (Maher et al., 2013). At neutral-alkaline pH, the carbonate complexes $UO_2(CO_3)_2^{2-}$ and $UO_2(CO_3)_3^{4-}$ are the predominant species. Uranyl carbonate complexes have a lower diffusion coefficient (5.6×10^{-10} m^2s^{-1}) than that of hydrated uranyl ions (7.6×10^{-10} m^2s^{-1}) (Grenthe et al., 1992) and an equatorial U–O bond length that is marginally longer (2.43 Å) than that of hydrated uranyl ions (2.41 Å) (Kalintsev et al., 2023). In the tricarbonate uranium complex, the U–C (carbonate) bond length is approximately 2.90 Å, and the U–C–O (distal carbonate oxygen) is around 4.15 Å. The formation of carbonate complexes has a considerable impact on the adsorption of uranium on mineral surfaces in natural processes (Maher et al., 2013; Gandhi et al., 2022), as well as on adsorbents used for uranium removal or capture in water treatment processes.

Under groundwater redox conditions, uranium complexes adsorb to mineral surfaces through covalent or hydrogen bonding and hydrophobic interactions, while reversible adsorption occurs via van der Waals forces and electrostatic interactions (Silva and Nitsche, 1995). The specific interactions during U(VI) adsorption involve outer-sphere surface complexation of U(VI) with N- and O-based functional groups (weak electrostatic interaction of the hydrated ion with the surface) (Zou et al., 2017), inner-sphere surface complexation of U(VI) with oxygen-containing functional groups (strong direct bonding with the surface upon partial dehydration) (Zong et al., 2013b), chelation with hydroxyl, carboxylic, or amino groups (Bayramoglu and Arica, 2016), ion exchange with various cations (Wang et al., 2018), electrostatic interactions with various charged groups (Kong et al., 2016; Zou et al., 2017; Wang et al., 2018), cation-π interaction between U(VI) and hydroxyl and carboxyl groups (Wang et al., 2022), and precipitation or reduction to sparsely soluble U(IV) (Kong et al., 2016; Zou et al., 2017). A cation exchange mechanism is significant at acidic to circumneutral pH and low ionic strength (≤10 mM), whereas inner-sphere surface complexation prevails at neutral to alkaline pH and high ionic strength (≥1 M) (Khan et al., 2021).

In the presence of cations and carbonate, the uranyl ion can form a series of neutral, anionic, and polynuclear species that influence uranium adsorption on mineral surfaces (Maher et al., 2013), such as zeolites (Davis and Randall, 2001; Nekhunguni et al., 2017). Carbonate species of uranium play an important role in the adsorption of U(VI) on adsorbents. When $UO_2(CO_3)_2^{2-}$ and $UO_2(CO_3)_3^{4-}$ dominate in solution, the uranium adsorption on iron oxide adsorbent is decreased (Ching-kuo Daniel and Langmuir, 1985; Nekhunguni et al., 2017).

Selective removal of U(VI) from water can be achieved through nanofiltration (NF) membranes, which retain over 95% of $UO_2(CO_3)_2^{2-}$ and $UO_2(CO_3)_3^{4-}$ (Raff and Wilken, 1999). Multiple mechanisms, including solution-diffusion, size exclusion, charge interaction, and adsorption, contribute to uranium removal via NF membranes (Shen and Schäfer, 2014). However, NF can be limited by solute diffusion due to concentration polarization at high pressures (Shen and Schäfer, 2014). Composite membranes with superior uranium adsorption can be prepared by integrating adsorbent materials. Rapid adsorption rates are necessary to maintain high flow rates and reduce processing times (Hao et al., 2021). Such membranes should maintain high adsorption efficiency over multiple cycles of use and regeneration. Integrating adsorbent materials like aluminosilicates into the membrane may enhance uranium retention at lower pressures. Zeolites, with their unique properties, offer significant potential for use in composite membrane

applications.

Zeolites are natural or synthetic hydrated aluminosilicates composed of $(SiO_4)^{4-}$ and $(AlO_4)^{5-}$ tetrahedra, forming a negatively charged porous network with pore sizes ranging from 3 and 8 Å (Baerlocher et al., 2007). Their distinct features—such as pore size, shape, topology, extra-framework cations, and Si/Al ratio—give zeolites unique ion removal and adsorption properties (Xie et al., 2019; Vasconcelos et al., 2023). With high cation exchange capacity, large surface area, micropore volume, and low cost, zeolites are widely used in separation and purification due to their size-sieving, diffusion-controlled, and adsorptive properties (Li et al., 2022b; Mahdavi Far et al., 2022; Yue et al., 2022). Various types of zeolites exhibit high uranium removal capacity, as summarized in Table 1.

Based on pore aperture diameters, zeolites can be classified into four types (Nazir et al., 2020): (i) small-pore zeolite with a pore diameter of around 4 Å such as Zeolite A (LTA) and chabazite (CHA), (ii) medium-pore zeolite frameworks with 5–6 Å pore sizes such as ZSM-5 (MFI) and ferrierite (FER), (iii) large-pore zeolites with 7 Å pore size such as Beta (BEA) and Faujasite (FAU), and (iv) extra-large-pore zeolites with pores over 7 Å such as CIT-5 (CFI) and ITQ-33 zeolites. Zeolites with large cavities and channels are ideal for uranium removal because relatively large cations, such as uranyl ions, can be accommodated (Fatima et al., 2013; Li et al., 2020b). The large-pore zeolites FAU and BEA further have a large surface area (800–1050 m^2/g), pore-free volume (370–2800 $Å^3$/unit cell), and porosity (9–18%) (Ektefa et al., 2022), which makes this type interesting candidates for adsorbing metal ions, such as uranium.

Changing the Si/Al ratio of the zeolite generally affects the amount and distribution of Si–O–Al groups in the crystal structure of zeolites (Su et al., 2012) and various properties (Li et al., 2023). The Si/Al ratio can be manipulated by desilication or the dealumination of zeolite (Graça et al., 2018; Li et al., 2023) to vary the nature of uranium binding. The tetrahedrally coordinated Al atoms create negative charges in the framework balanced by extra-framework cationic species. A zeolite with a low Si/Al ratio (high Al content and more negative charges) is expected to exhibit higher metal uptake due to increased electrostatic attraction and the abundance of ion exchange sites. Nevertheless, if chemisorption prevails over the ion exchange process, the Si/Al ratio becomes less significant in the case of some zeolites (Król et al., 2016). Additionally, water chemistry factors such as pH and competing ions also influence uranium removal efficiency (Camacho et al., 2010; Zou et al., 2011; Fatima et al., 2013).

The negatively charged sites of the porous network of zeolite are usually balanced by alkaline or alkaline earth metal cations, which can be replaced by other metals to enhance adsorption properties (Jiménez-Reyes et al., 2021). Transition metals like Cu, Fe, and Ni, as well as noble metals such as Pt and Pd, have been introduced into zeolites to improve adsorption and catalytic functions (Zhang et al., 2023). In particular, zeolites coated with iron oxides have been used to remove metallic contaminants from water, as they have a large surface area and affinity for metal ions (Nah et al., 2006; Han et al., 2009; Nekhunguni et al., 2017). Particularly, the uranium ion is known to have a high affinity for Fe oxides (Ching-kuo Daniel and Langmuir, 1985), which may assist uranium adsorption.

Fe incorporation into zeolites produces various Fe species, such as binuclear Fe–O–Fe cations, Fe_xO_y clusters, oxide particles, and isolated Fe ions (Maier et al., 2012). Fe-Beta Polymorph A zeolite contains isolated or binuclear Fe ions at exchange positions, small Fe_xO_y clusters, and large Fe_2O_3 particles on the surface that can enhance uranium adsorption. (Iwasaki et al., 2008; Maier et al., 2012). At pH < 5.5, uranyl ions directly bond to the hydrous ferric oxide surface as mononuclear bidentate inner sphere complexes (Waite et al., 1994). The predominant structure for U(VI)-carbonate ternary complexes formed on iron oxide is Fe–O–U(VI)-$(CO_3)_x$, where U(VI) bonds directly to the Fe oxide surface (hydr)oxo sites, while the carbonate ligands point away from the oxide surface (Davis and Randall, 2001; Nekhunguni et al., 2017).

Due to the intricate nature of zeolite-uranium interactions, identifying potential adsorption complex formations through geochemical modeling can improve the understanding of uranium removal mechanisms. Geochemical models like MINTEQA2, HYDRA/MEDUSA, EQ3/6, and SOLMINEQ.88 can predict speciation and sorption processes when adsorbent properties are not well characterized or data is limited (Damiania et al., 2015). PHREEQC, a geochemical modeling software, can estimate speciation, sorption, and species transport by adjusting variables like surface area and dosage, which might be costly or time-consuming to test experimentally (Parkhurst and Appelo, 2013). For instance, PHREEQC can model uranium reactions with $Al(OH)_n$ and $Si(OH)_n$ sites in zeolites with varying Si/Al ratios and Fe oxide (hydr)oxo sites using known or optimized equilibrium constants (log k).

While the use of iron oxide-modified zeolite has been reported for uranium adsorption (Nekhunguni et al., 2017), its application in filtration through zeolite-loaded membranes remains unexplored. Incorporating adsorbents into membranes enhances uranium contact and mass transfer for improved adsorption. This study explores iron-modified zeolite and composite membranes, combining the advantages of adsorption and filtration for better uranium removal. Microporous membranes with a nominal pore size of 0.45 μm were used to load zeolite particles, which were slightly smaller than the membrane's pore. Ultrafiltration membranes placed beneath the MF membrane were used to prevent zeolite leaching into the permeate in the event of desorption from the MF membrane. PHREEQC modeling offers preliminary insight into uranium speciation and its response to chemical conditions,

Table 1
Various types of zeolites reported for uranium removal.

Zeolite type	Frame-work (Baerlocher et al., 2007)	Channel diameter (A°)	Si/Al ratio	Extra-framework cation	Surface area (m^2/g)	Micropore volume (cm^3/g)	Uranium adsorption capacity (mg/g)	Uranium initial conc. (mg/L)	Ref.
Zeolite Y	FAU	8	2.6	Na	362	0.118	14–16	10–100	(Fatima et al., 2013; Li et al., 2020b)
Clinoptilolite	HEU	–	5.0	–	18–165	0.027	5–11	5–90	(Kilincarslan and Akyil, 2005; Camacho et al., 2010; Zou et al., 2011)
MnO_2 coated clinoptilolite	–	–	–	–	24–28	–	13–18	50–120	Zou et al. (2009)
ZnO clinoptilolite	–	–	5.69		70	0.005	5.8	8.3	Aghadavoud et al. (2016)
Zeolite A	LTA	5	–	Na	342	0.123	1.0–6.5	10–100	Nibou et al. (2011)
Zeolite X	–	–	–	–	–	–	252	11.8	Olguí;n et al. (1999)
CuO modified zeolite X	–	–	–	–	–	–	9	200	Abdi et al. (2014)
4A zeolite	LTA	4.1	–	–	–	0.16	8.5–32	5–100	Barkat et al. (2015)
P1 zeolite	GIS	3.1	–	–	–	0.17	8.3–100	5–100	Barkat et al. (2015)

enabling a more tailored approach to water treatment processes. The following research questions are investigated for uranium adsorption with zeolite; i) How uranium uptake by zeolite changes with speciation (pH) and competing ions (ionic strength), ii) Whether removal is limited by zeolite loading and hydraulic residence time in the zeolite/MF/UF composite, and iii) If zeolite-loaded membranes improve mass transfer over static adsorption.

2. Materials and methods

2.1. Zeolites types and properties

Commercial zeolites of the frameworks Faujasite (FAU) and Beta polymorph A (BEA) with different metals and Si/Al ratios were used for the uranium removal studies. FAU-type zeolites used were NaY (Alfa Aesar, Germany), HY CBV 720, HY CBV 780 (Zeolyst International, The Netherlands) and LiCZF2 (Clariant Produkte GmbH, Germany). BEA-type zeolites used were HCZB 30, HCZB150, and FeCZB30 (Clariant Produkte GmbH, Germany). The different types of zeolites used in this study and their characteristics are listed in Table 2.

FeCZB30 used for the adsorption and filtration studies possessed a BET surface area of 627 m^2/g, Al wt% 0.68, SiO_2 wt% 20.88 and Fe_2O_3 wt% 3.23 as reported by the manufacturer. In addition to the zeolite listed in Table 2, modified NaY was used in addition for preliminary adsorption experiments. The NaY zeolite was modified for desilication and dealumination to manipulate the Si/Al ratio, following published procedures (Tarach et al., 2017; Graça et al., 2018). For desilication, 8 g of NaY zeolite was heated in 250 mL of 0.8 M NaOH at 60 °C for 2 h in a conical flask on a hot plate (VMS-C7, VWR, Germany). For dealumination, 6 g was heated in 150 mL of 0.2 M HNO_3 at 60 °C. In the second step, the suspension was cooled in an ice bath at 0−5 °C (Alpha RA24, Lauda, Germany) for 10 min and filtered with a 0.2 μm filter (GVPP PVDF, Millipore, USA). The cake deposit on the filter was washed with MilliQ water until a neutral pH was obtained and subsequently dried in a Petri dish in a hot air oven (FD 53, RS 422 interface, Binder, Germany) at 100 °C for at least 16 h. The dried, desilicated, or dealuminated zeolite obtained in hydrogen form was ground into fine particles in a mortar. The procedure was repeated to convert the modified samples into sodium form by heating the modified zeolite in 1 M $NaNO_3$ in a conical flask on a hot plate. All the steps from cooling to grinding in the mortar were followed as given above to obtain the sodium form of desilicated and dealuminated zeolites. The samples modified from zeolite NaY (FAU-Na1) were abbreviated as follows: desilicated (hydrogen form) (FAU-H0), desilicated and dealuminated (hydrogen form) (FAU-H1), desilicated (sodium form) (FAU-Na0), and desilicated and dealuminated (sodium form) (FAU-Na2).

2.2. Preparation of a zeolite-loaded composite membrane and filtration protocol

A microfiltration membrane (MF, 0.45 μm, nitrate cellulose, Sartorius, India) was used for zeolite incorporation. The pore size of these membranes were similar to the zeolite size and offered both the surface area and pore volume for zeolite loading. These zeolite-loaded MF membranes were then placed onto an ultrafiltration (UF, MWCO 300 kDa, PBMK BioMax, Millipore, USA) membrane to prevent the zeolite from leaching into the permeate in case of desorption from the MF membrane.

The selected MF and UF membranes were demonstrated to have lower uranium adsorption than the MF membranes GVPP PVDF 0.2 μm (Millipore, USA) and the UF membrane PLHHK 100 kDa (Millipore, USA) used in the control experiments without zeolite, as shown in Fig. S7.

Zeolite loading was carried out in a stainless steel (SS) stirred cell of 900 mL with a filtration area of 38.5 cm^2 at 400 rpm and 20 ± 3 °C. The filtration protocol was adapted from previous reports (Imbrogno and Schäfer, 2019; Boussouga et al., 2023). The MF/UF stack was first wetted by filtering with MilliQ water, followed by a pure water permeability measurement. Suspensions with varying weights of zeolite (0.1–1.0 g) were then filtered through the MF/UF stack at a 1 L/h flow rate for surface and pore loading of zeolite.

2.3. Uranium properties and solution chemistry

Uranium stock solution was prepared from hydrated uranyl chloride ($UO_2Cl_2.3H_2O$, purity 99.9%, IBILABS, USA). The multi-element standard solution (Certipur, ICP multi-element standard solution VI) used for calibration of ICP-MS was purchased from Merck, Germany.

A background solution containing 10 mM NaCl and 1 mM $NaHCO_3$ (VWR chemicals, Germany, 99.9% purity) was prepared for all experiments. The pH was adjusted using 1–3 M solutions prepared from HCl (36%, VWR) and NaOH pellets (AnalaR, purity 99.9%, Merck). 65% HNO_3 (Merck, purity 99.9%) was used to acidify samples for ICP-MS analysis. All solutions were prepared in Milli-Q water (MilliQ A+ system, Millipore, Germany).

2.4. Static adsorption experiments

Varying amounts of zeolite according to the desired concentrations (0.1–2.0 g/L) were measured using an analytical balance (AC 210P, Sartorius, Germany) and transferred into 250 mL conical flasks containing 250 mL of 10 mM NaCl and 1 mM $NaHCO_3$ background electrolyte solution. The zeolite suspension was shaken for an hour in a shaker (Innova 43 R, New Brunswick Scientific, USA) at 260 rpm at

Table 2
Properties of the zeolite types.

Types of zeolite	Code used	Framework (Baerlocher et al., 2007)	Crystal chemical data (Baerlocher et al., 2007)	Channel diameter (Å)[a]	Si/Al ratio[a]	Surface area (m^2/g)[a]	Particle size (nm)[b]
Zeolite NaY	FAU-Na1	FAU	$[Na_{58}(H_2O)_{240}][Al_{58}Si_{134}O_{384}]$	7.4	1.3	934	350 ± 170
Zeolite Y, Hydrogen (CBV 720)	FAU-H30	FAU	$[Na_{58}(H_2O)_{240}][Al_{58}Si_{134}O_{384}]$	7.0	30	–	462 ± 290
Zeolite Y, Hydrogen (CBV 780)	FAU-H80	FAU	$[Na_{58}(H_2O)_{240}][Al_{58}Si_{134}O_{384}]$	7.0	80	–	582 ± 410
LiCZF2	FAU-Li2	FAU	$[Na_{58}(H_2O)_{240}][Al_{58}Si_{134}O_{384}]$	8.0	2	>600	576 ± 330
HCZB 30	BEA-H30	BEA	$Na_7[Al_7Si_{57}O_{128}]$	7.0	30	>500	341 ± 101
HCZB 150	BEA-H150	BEA	$Na_7[Al_7Si_{57}O_{128}]$	7.0	150	>500	314 ± 90
FeCZB30	BEA-Fe30	BEA	$Na_7[Al_7Si_{57}O_{128}]$	7.0	30	627	420 ± 80

[a] As reported by the manufacturer.
[b] From DLS measurements.

20 °C to ensure good mixing. The pH of the suspension was measured and adjusted with 1 M HCl or NaOH. A 1 g/L uranium solution was then added to this zeolite suspension to attain a uranium concentration of 250 μg/L and shaken for 26 h.

The pH of uranium solutions was varied from 2 to 12 to investigate the role of speciation, and the ionic strength was varied from 0.6 to 20.0 g/L NaCl (corresponding to a wide salinity distribution of brackish groundwater (Li et al., 2020a)) to investigate the contribution of salinity to uranium removal. A 6-mL sample was drawn with a micropipette into centrifuging tubes at different intervals (0, 15, and 30 min and 1, 2, 4, 6, 22, 24, and 26 h) for immediate centrifugation at 4000 rpm (Sigma 3–16L, Sigma Laborzentrifugen GmbH, Germany) for 20 min. The centrifugation time was optimized, details are provided in Fig. S2.

2.5. Filtration of uranium through a zeolite-embedded MF/UF stacked membrane

Uranium filtration through the zeolite-embedded composite membranes was performed in a dead-end filtration cell following a protocol adapted from a previous report (Boussouga et al., 2022) (see Fig. S1). 250 μg/L uranium in 10 mM NaCl and 1 mM $NaHCO_3$ background electrolyte solution was filtered through the zeolite-loaded MF/UF membrane (Fig. 1), and permeate samples were collected at different permeate volumes (20, 40, 60, 80, 100, 200, 300, 400, 500, 600, 700, and 800 mL).

2.6. Uranium removal efficiency and adsorption kinetics

The percentage of U(VI) removal by zeolite at specific times throughout the experiment was calculated with Equation (1);

$$R_t = \frac{c_0 - c_t}{c_0} \cdot 100 \quad (1)$$

where c_0 is the initial uranium concentration (μg/L) before adsorption and c_t is the concentration (μg/L) of the centrifugate or supernatant at time t. The uranium uptake q_t (μg/g) on zeolite by static adsorption at a specific time was calculated using Equation (2).

$$q_t = \frac{c_0 - c_t}{m} \cdot V \quad (2)$$

where m is the mass of zeolite (g) at a time (t) and V is the volume of supernatant (L).

The uranium uptake q_t (μg/g) on zeolite by filtration at a specific time was calculated using Equation (3).

$$q_t = \frac{c_{f\bullet} V_f - \Sigma\, c_{p\bullet} V_p - c_{c\bullet} V_c}{m} \quad (3)$$

where c_f, c_p, and c_c is the concentrations (μg/L) of feed, permeate, and concentrate, and V_f, V_p, and V_c the corresponding volume (L) of feed, permeate, and concentrate at time (t), m is zeolite mass (g).

The kinetics of adsorption determined in static adsorption were compared using the pseudo first-order (PFO), pseudo second-order (PSO), and Elovich kinetic models (Largitte and Pasquier, 2016). These kinetic models offer unique perspectives on adsorption kinetics. The PFO model postulates that the rate of adsorption is directly linked to the number of available sites, making it suitable for liquid-phase adsorption scenarios. In contrast, the pseudo second-order model, suggests that the rate is related to the square of the number of unoccupied sites, hinting at a chemisorption process. The Elovich model, which is often used for chemisorption on heterogeneous surfaces, describes a scenario where the adsorption rate decreases exponentially as the amount of adsorbate increases. Based on the heterogeneous nature of zeolite surfaces, and the empirical fit of these models to the experimental data, PFO and Elovich kinetic models were chosen for discussion. A thorough explanation of the assumptions and implications of both the PFO and Elovich models is included in the Supporting Information. The PFO model is provided in equation (4);

$$q_t = q_e\left(1 - e^{-k_1 \bullet t}\right) \quad (4)$$

where k_1 is the rate constant in h^{-1}, q_t is the uptake at t, and q_e is the equilibrium uptake in μg/g. The Elovich model (Largitte and Pasquier, 2016) is given by equation (5);

$$q_t = \frac{1}{\beta}\ln(\alpha \bullet \beta \bullet t + 1) \quad (5)$$

where α is the initial sorption rate in $\mu g.g^{-1}.min^{-1}$ and β is constant related to the extent of surface coverage and activation energy for chemisorption in $g.\mu g^{-1}$.

The estimation of absolute and relative errors for uranium removal, uptake, and membrane permeability is described in Table S3, based on the method adapted from Imbrogno et al. (2024).

2.7. Water quality analysis

Solution pH and electrical conductivity were measured using a multiparameter portable meter (pH/Cond 3320, WTW, Germany) with pH (SenTix® 41, WTW, Germany) and conductivity (WTW TetraCon 325, Germany) sensors.

Inductively coupled plasma mass spectrometry (ICP-MS) (Agilent,

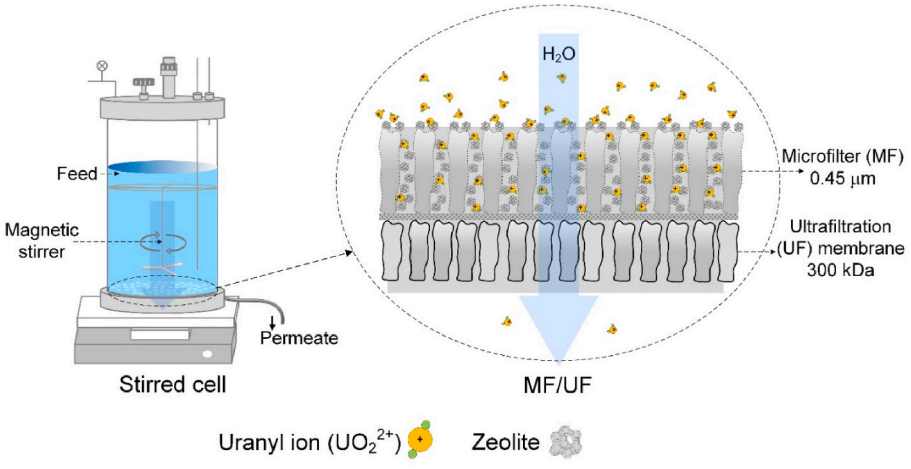

Fig. 1. Schematic of a zeolite-embedded microfilter (MF)/ultrafiltration (UF) stacked membrane within a stirred cell.

model J8403A 7900 ICP-MS, Japan) was used to measure the uranium concentration of samples. The uranium concentration of stock solutions was verified with the ICP multi-element standard (ICP standard solution VI 30 elements, 9.9 ± 0.5 mgU/L, Certipur®, Germany). Concentration calibration was performed using standard solutions of serial concentrations in the range of 0.25–1000 μgU/L prepared from a 2 mgU/L stock solution. Before analysis, the samples and standard solutions were acidified in 2% (w/w) HNO_3 (Merck, Suprapur 65%, Germany). Calibrations and the limit of detection (LoD) are included in Fig. S4. The interference on ICPMS signal of uranium by high salt concentration was corrected in the calibration (Fig. S5).

2.8. PHREEQC modeling

The PHREEQC interactive geochemical modeling code version 3.7.3-15968 (USGS, 2021) was used to identify the speciation of uranium upon its adsorption to $Al(OH)_n$, $Si(OH)_n$, and $Fe(OH)_n$ sites in zeolite aqueous solutions at different conditions. The Wateq4f.dat inbuilt database was used to simulate the PHREEQC input scripts (Mosai et al., 2021), which helps to identify changes in uranium interaction at low or high pH. Surface simulations were based on the diffuse double-layer surface-complexation (DDL) model by Dzombak and Morel (1990) (Dzombak and Morel, 1990). The surface reactions of the major uranium species and the active surface sites with their equilibrium constants (log k) used for PHREEQC simulation are listed in Table 3.

The assumptions adopted for modeling surface interaction in PHREEQC are listed in the supporting information, including model parameters used to calculate the total binding sites of the adsorbent (Table S8), the calculated number of sites for the different Si/Al ratios (Table S9), PHREEQC input parameters (Table S10), the definition and keywords used for PHREEQC simulation (Table S11), and the equilibrium constants for different minerals of SiOH and AlOH and uranium species (Table S12).

2.9. Membrane and zeolite nanoparticle characterization

The surface morphology of pristine zeolite particles, as well as the surface and cross-sectional morphology of zeolite-loaded composite membranes, were examined using a scanning electron microscope (SEM, Supra 60VP equipped with SE-ll detector, Zeiss, Germany). A suspension of pristine zeolite particles was drop-cast using a method adapted from a previous report (Boussouga et al., 2023). A 800 mg/L suspension of pristine zeolite was prepared by shaking 4 mg of each zeolite sample in 5 mL of Milli-Q water in Eppendorf tubes, followed by 3 h of sonication. 50 μL drops of the prepared solution was placed onto the SEM support (flat ⌀ 12.5 mm, G301D, Plano-em, Germany), covered with double-sided carbon tape (12 mm · 5 m roll, G3349C, Plano-em, Germany). The drops were then dried at room temperature (20 ± 1 °C).

Zeolite-loaded and pristine membranes were cut into small sections for surface and cross-sectional SEM imaging. 1·1 cm sections were cut from membrane coupons using a sharp sterile stainless-steel blade (05XX, Swann-Morton, England) for the top view imaging. The cross-section membrane samples for SEM evaluation were prepared using a Cryomicrotome (CM-1860UV, Leica, Germany). Before sectioning, the membrane sample was frozen in a tissue freezing medium (Leica) at −30 °C. The sample was then cut with a low-profile microtome blade (DB80LX, Leica, Germany), the cross-section samples were then washed and soaked in Milli-Q water for about 15 min to remove the freezing gel and dried at 20 ± 1 °C for 24 h. Prior to the SEM imaging, the pristine zeolite particles and membrane samples were coated with a thin layer of gold (25 nm) using a sputter coating system (SCD 005, BAL-TEC, Germany) to enhance the conductivity of the samples.

The crystal structure of the pristine zeolites framework (FAU and BEA) was analyzed by X-ray diffraction (XRD) (Fig. S13). For XRD analysis, the powdered zeolite samples were filled into the circular sample XRD holder and loaded into the XRD machine (XRD, D2 Phaser, Bruker AXS GmbH, Germany) equipped with CuKα (l = 1.54184 Å) radiation operated at a voltage of 30 kV and a current of 10 mA.

Table 3
Surface reactions of the major uranium species and the active surface sites used for PHREEQC simulation.

No.	Surface reactions	Log k constants	Reference
1	$Surf\_alOH + H^+ = Surf\_alOH_2^+$	12.30	Zachara and McKinley (1993)
2	$Surf\_alOH = Surf\_alO^- + H^+$	−13.16	Zachara and McKinley (1993)
3	$Surf\_alOH + UO_2^{2+} = Surf\_alOUO_2^+ + H^+$	1.40	Guo et al. (2009)
4	$Surf\_alOH + 2UO_2^{2+} + CO_3^{2-} + 3H_2O = Surf\_alO(UO_2)^2CO3(OH)_3^{2-} + 4H+$	0.99	Guimarães et al. (2016)
5	$Surf\_siOH + H^+ = Surf\_siOH_2^+$	−0.95	Turner et al. (1996)
6	$Surf\_siOH = Surf\_siO^- + H^+$	−6.90	Östhols (1995)
7	$Surf\_siOH + UO_2^{2+} = Surf\_siOUO_2^+ + H^+$	0.99	Korichi and Bensmaili (2009)
8	$Surf\_siOH + UO_2OH^+ = Surf\_siOUO_2OH + H^+$	1.00	Bachmaf and Merkel (2011)
9	$Surf\_siOH + UO_2(CO_3)_3^{4-} = Surf\_siOHUO_2(CO_3)_3^{4-}$	8.00	Bachmaf and Merkel (2011)
10	$Surf\_siOH + UO_2(OH)_3^- = Surf\_siOHUO_2(OH)_3^-$	6.90	Bachmaf and Merkel (2011)
11	$Surf\_feOH + H^+ = Surf\_feOH_2^+$	7.47	Lövgren et al. (1990)
12	$Surf\_feOH = Surf\_feO^- + H^+$	−9.51	Lövgren et al. (1990)
13	$Surf\_feOH + UO_2^{2+} = Surf\_feOUO_2^+ + H^+$	5.20	Mahoney et al. (2009)
14	$Surf\_feOH + UO_2^{2+} + CO_3^{2-} = Surf\_feOUO_2CO_3^- + H^+$	7.55	Wazne et al. (2003)

3. Results and discussion

Static adsorption of uranium on zeolite was performed at varying conditions for different zeolite types, amounts, and solution chemistry conditions. Before implementing zeolite-loaded MF/UF membranes for uranium filtration, the kinetics and isotherms of zeolite-uranium adsorption were examined to understand the adsorption processes. In the first instance, a static adsorption experiment was conducted to determine which zeolites exhibited the greatest capacity for uranium adsorption.

3.1. Uranium adsorption by zeolites

The interaction of uranium with zeolite depends on the nature and type of zeolite. Several commercial zeolites of FAU and BEA types with various metal substitutions (H, Na, Li, and Fe forms) and variable Si/Al ratios in the range 5–150 (see Table 2) were utilized to determine appropriate zeolites for uranium removal from aqueous solution. Prior research on U(VI) sorption has demonstrated that the pH of the solution is a critical factor that influences the sorption process (Nekhunguni et al., 2017; Boussouga et al., 2024). PHREEQC simulation was carried out at the adsorption experimental conditions of 250 μg U/L, 10 mM NaCl and 1 mM $NaHCO_3$ background electrolyte concentration, and 20 °C to understand the uranyl aqueous speciation with pH (see Fig. 6D for speciation). The free uranyl UO_2^{2+} ion was found to be the dominant species in the acidic pH range up to pH 5, which is in agreement with previously reported results (Arnold et al., 2001; Bachmaf and Merkel, 2011; Nekhunguni et al., 2017; Boussouga et al., 2024).

Consequently, uranium adsorption experiments were carried out at pH 4 to investigate the role of various zeolites on uranyl ion removal (Fig. 2). As anticipated, uranium concentration in the adsorbate solution changed with the zeolite type used. Zeolites with a high Si/Al ratio typically exhibit the highest uranium removal at pH 4. All the BEA-type zeolites (BEA-H30, BEA-H150, and BEA-Fe30) and some FAU types

(FAU-H30 and FAU-H80) showed the lowest uranium concentration in the solution. WHO guideline (30 μg/L U) was met within 60 min of adsorption (32.5 μg/L U) when using Fe-incorporated BEA zeolite (BEA-Fe30).

A high Si/Al ratio (high silica) condition is commonly regarded as unfavorable for uranium adsorption by ion exchange mechanisms (Król et al., 2016). In the case of BEA zeolite, a high-silica condition typically denotes Si/Al ratios exceeding 10, in contrast, in the case of FAU, it indicates Si/Al ratios exceeding 3 (Li et al., 2023). Since all zeolites with high uranium removal in the adsorption experiment have a high silica content and therefore fewer cation exchange sites, it can be inferred that ion exchange is likely not the major factor contributing to uranyl ion adsorption presented in Fig. 2. Zeolites with higher Si/Al ratios possess more uniform and well-defined stable pore structures with large surface areas, which facilitate the diffusion and uptake of uranium ions more effectively. The increased hydrothermal stability of these zeolites ensures they retain their structural integrity, allowing for more reliable and sustained adsorption performance, even under aggressive environmental conditions (Aytas et al., 2004). It has been observed that zeolites with a high Si/Al ratio, such as pentasils, can adsorb metals by forming stable inner-sphere complexes via the chemisorption process. Chemisorption occurs as the functional groups of aluminosilicate networks, especially OH groups, form strong chemical bonds with metal ions without a hydration layer (Król et al., 2016).

A PHREEQC simulation was used to study the effect of varying Si/Al ratios on uranium removal at different pHs (Fig. 3). The PHREEQC results demonstrated that the removal of uranium increased as the Si/Al ratio increased from 1 to 300 in the alkaline solution. The adsorption of uranium was strongly dependent on solution pH. High removal is observed at pH between 4 and 9 while there was a clear decrease in uptake as pH increased from 10 to 12. There is no appreciable difference in uranium removal when the Si/Al ratio >300. Based on the PHREEQC simulation, an Si/Al ratio of 30 and a pH of 8 were chosen for further adsorption experiments. Fe-incorporated zeolite of Si/Al ratio 30 exhibited one of the most significant uranium removals, and zeolites containing Fe exhibit diverse interactions with metal ions, including uranium (Ching-kuo Daniel and Langmuir, 1985). As a consequence, BEA-Fe30 was chosen for further uranium adsorption investigation.

3.2. *Quantity of Fe-zeolite required for uranium removal*

Static adsorption experiments were performed on 250 μg/L uranium at different concentrations (0.1–2.0 g/L) of BEA-Fe30 to estimate the minimum amount of zeolite required for removing uranium from the solution (Fig. 4).

Nearly complete removal of uranium is observed at zeolite concentrations of 0.6 g/L and above. This indicates that BEA-Fe30 has a high surface area, offering a large number of adsorption sites. At dosages higher than 0.6 g/L, the additional zeolite does not further remove uranium because the excess adsorption sites remain unoccupied,

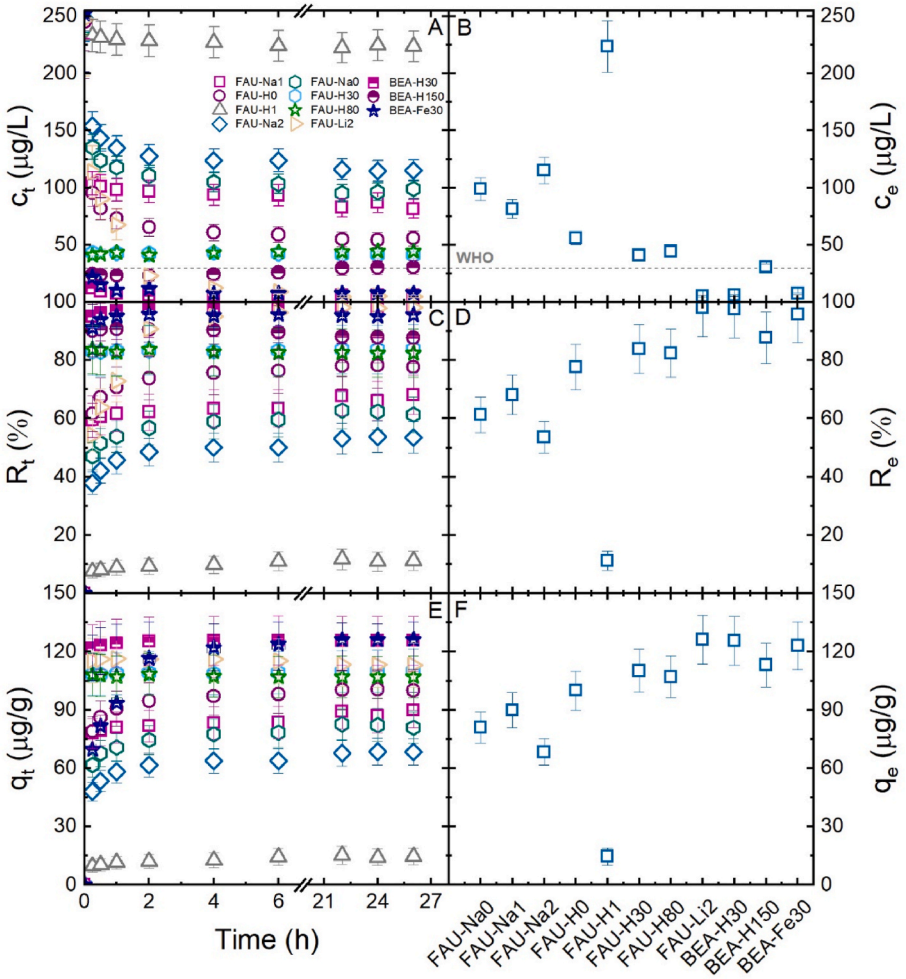

Fig. 2. (A) Uranium concentration in adsorbate solution (C) uranium removal (E) adsorptive capacity as a function of time; (B) Uranium equilibrium concentration (D) Equilibrium removal and (F) Equilibrium adsorptive capacity with a 2.0 g/L suspension of different zeolites. Initial uranium concentration: 250 μg/L, pH: 4.0 ± 0.1, 1 mM $NaHCO_3$, 10 mM NaCl, 20 °C, 260 rpm.

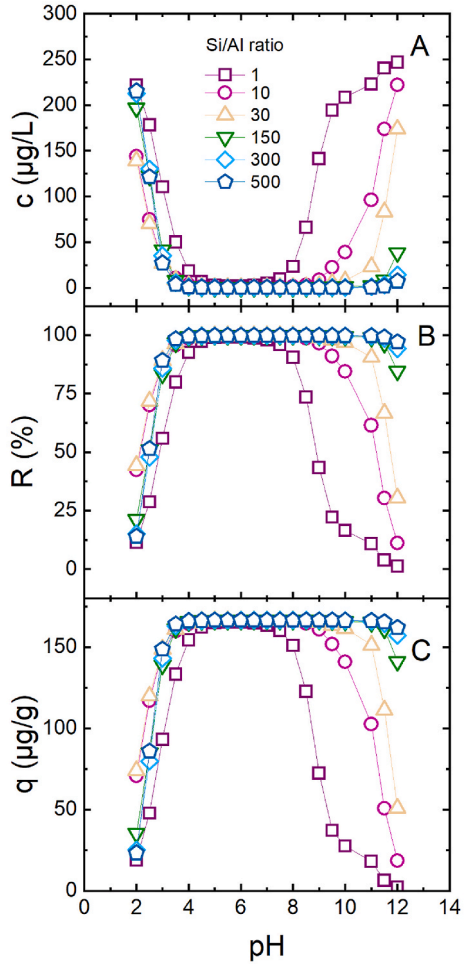

Fig. 3. PHREEQC simulation of (A) Uranium concentration in adsorbate solution, (B) uranium removal and (C) uranium uptake as a function of pH at various Si/Al ratio. Zeolite dosage 2 g/L, initial uranium concentration 250 µg/L, 1 mM $NaHCO_3$, 10 mM NaCl and 20 °C, modelled with the wateq4f database.

showing an excess of available sites relative to the amount of uranium. The WHO guideline concentration is achieved with 0.6 g/L Fe-zeolite within 1 h. The lower the zeolite concentration, the more time is required to achieve the WHO guideline concentration.

The uranium uptake decreased exponentially with zeolite concentration. Similar observations of a reduction in uranyl uptake with zeolite concentration have been reported for NKF-6 zeolite with a Si/Al ratio of 29 (Zong et al., 2013a). It could also be possible that an increased zeolite dosage enhances the likelihood of collisions between zeolite particles, potentially inducing particle agglomeration, which could reduce the overall surface area (Zong et al., 2013a). Although this factor might contribute to a decline in the adsorption capacity of uranium, this has not been observed from the adsorption data with zeolite concentrations 0.1−2 g/L in Fig. 4. However, DLS measurements indicate that the zeolite particles may indeed undergo agglomeration at high dosages (Fig. S12).

Studying the adsorption kinetics of uranium on zeolite at different loadings will help to understand how varying amounts of zeolite influence the rate and efficiency of uranium removal from water.

3.3. Adsorption kinetics in static adsorption

To elucidate the potential rate-determining steps and mechanisms of reaction, kinetic models were applied to the experimental data of batch adsorption. The PFO (Lagergren, 1898) and Elovich models were fitted to the kinetic data (Fig. 5). PFO (Sahoo and Prelot, 2020) is based on the assumption that the rate of adsorption is directly proportional to the number of unoccupied sites on the adsorbent surface. In contrast, the Elovich model (Largitte and Pasquier, 2016) implies that adsorption is not directly proportional to the number of unoccupied sites, and the energy of adsorption increases linearly with the surface coverage (Aharoni and Tompkins, 1970; Chien and Clayton, 1980). The Elovich model assumes that the adsorbent surface is heterogeneous, with adsorption sites of different energy levels. A detailed description of the model assumptions and the implications of both PFO and Elovich models are given in the Supporting Information (Section 6).

At lower zeolite loading (concentration <0.6 g/L), the uranium adsorption data fitted well for the Elovich model compared to the PFO model. The plausible explanation for the poor fitting at lower zeolite loading could be due to several reasons, such as surface heterogeneity (non-linear dependence on the number of low energy adsorption sites), and varying interactions of uranium with particular zeolite adsorption sites (Rudzinski and Plazinski, 2006; Sen Gupta and Bhattacharyya, 2011). The number of available sites for adsorption (indicated by β the Elovich model) increases exponentially with the zeolite concentration (Table S6). The low uptake, q_t (µg/g), and high surface availability, β (g/µg), at at high zeolite concentrations suggest that the uranium is completely adsorbed. At high zeolite loading (concentration at 0.6 g/L and above), both Elovich and PFO models fitted well ($R^2 \geq 0.98$ at and above 0.6 g/L zeolite) for the uranium adsorption. This is attributed to the fact that the number of available adsorption sites is much greater, potentially leading to more uniform adsorption behavior. When there are abundant adsorption sites relative to the uranium concentration, the system approaches a more uniform adsorption process. Both the Elovich and PFO models can describe such impact on the overall adsorption kinetics when abundant adsorption sites are available. Given the low concentration of uranium in the water, this appears plausible.

Understanding the adsorption kinetics of uranium on zeolite, particularly at different loadings, provided valuable insights into the mechanism of the uranium removal process, which is further influenced by the speciation of uranium under varying environmental conditions.

3.4. Speciation (pH) dependence of uranium adsorption

Uranium exists as positively charged uranyl ions below pH 5. PHREEQC simulations indicate that with increasing pH, U(VI) speciation is dominated by U hydrolysis products (UO_2OH^+ and $UO_2(OH)_3^-$) and carbonate species (UO_2CO_3, $UO_2(CO_3)_2^{2-}$, and $UO_2(CO_3)_3^{4-}$), which is in agreement with previously reported results (Bachmaf and Merkel, 2011; Coutelot et al., 2018). Static adsorption was carried out between pH 2 to 12 to understand the relationship between uranium speciation and zeolite adsorption behavior (Fig. 6).

Neutral and alkaline pH values show higher uranium removal, due to the changes in uranium speciation. WHO recommended concentration of uranium was achieved in the adsorbate (supernatant) solution only above pH 6. The fastest kinetics of uranium adsorption at pH 6 and 8 is indicated by the sharp decline of uranium concentration in the adsorbate solution. The uranium speciation (Fig. 6 D) estimated in PHREEQC using wateq4f database shows that uranyl cation (UO_2^{2+}) is the dominant species in the acidic pH range up to pH 5 which is in agreement with previous reports (Arnold et al., 2001; Bachmaf and Merkel, 2011). With increasing pH, U(VI) speciation is dominated by uranium hydrolysis products (UO_2OH^+ and $UO_2(OH)_3^-$) as well as carbonate complexes (UO_2CO_3, $UO_2(CO_3)_2^{2-}$ and $UO_2(CO_3)_3^{4-}$) which is consistent with literature (Bachmaf and Merkel, 2011; Coutelot et al., 2018). Negatively charged uranium species dominate above pH 6. At pH 7, $UO_2(CO_3)_2^{2-}$ is the dominant species, while between pH 8 and 10 $UO_2(CO_3)_3^{4-}$ becomes the major species. At pH values greater than 11, $UO_2(OH)_3^-$ is most abundant.

Very high uranium uptake of 125–130 µg/g is observed at pH 6–12 at equilibrium, decreasing to 111 µg/g at pH 4 and 3 µg/g at pH 2. The high

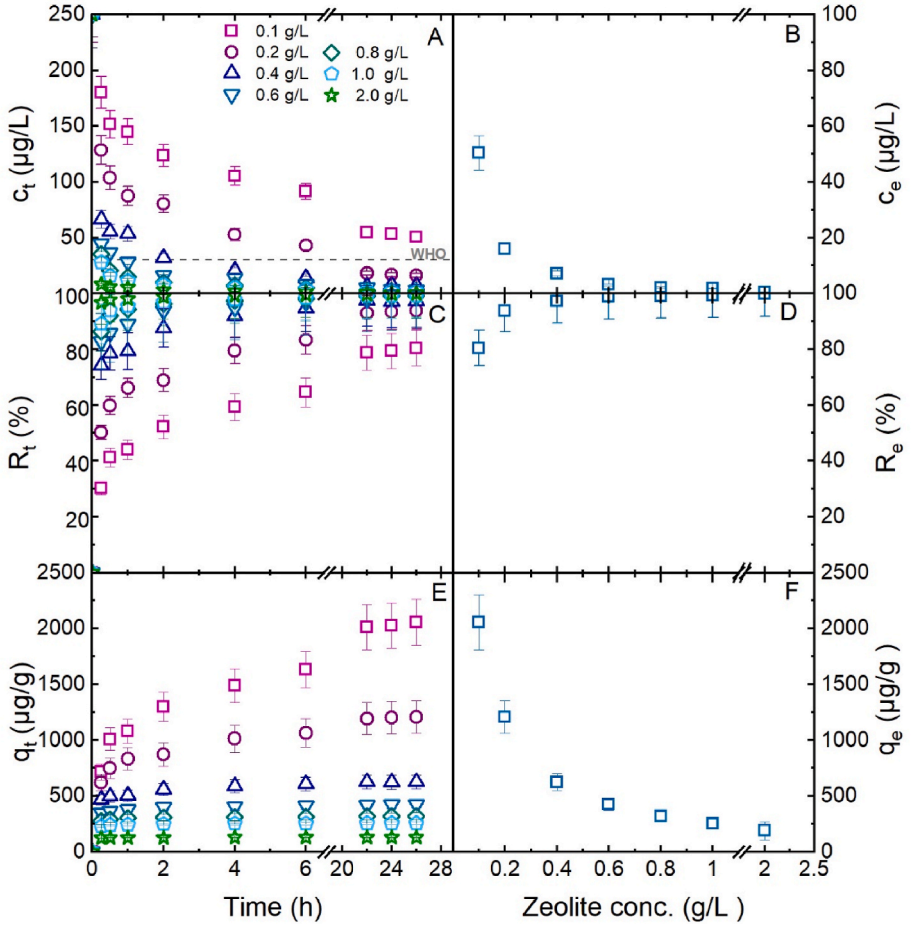

Fig. 4. (A) Uranium concentration in adsorbate solution; (C) Uranium removal; (E) Uranium uptake at 0.1–2.0 g/L BEA-Fe30 concentrations. The corresponding values at the equilibrium time (26 h) are shown on the right side (B, D, and F) as a function of zeolite concentration. Initial uranium concentration: 250 µg/L, pH: 8.0 ± 0.1, 1 mM $NaHCO_3$, 10 mM NaCl, 20 °C, 260 rpm.

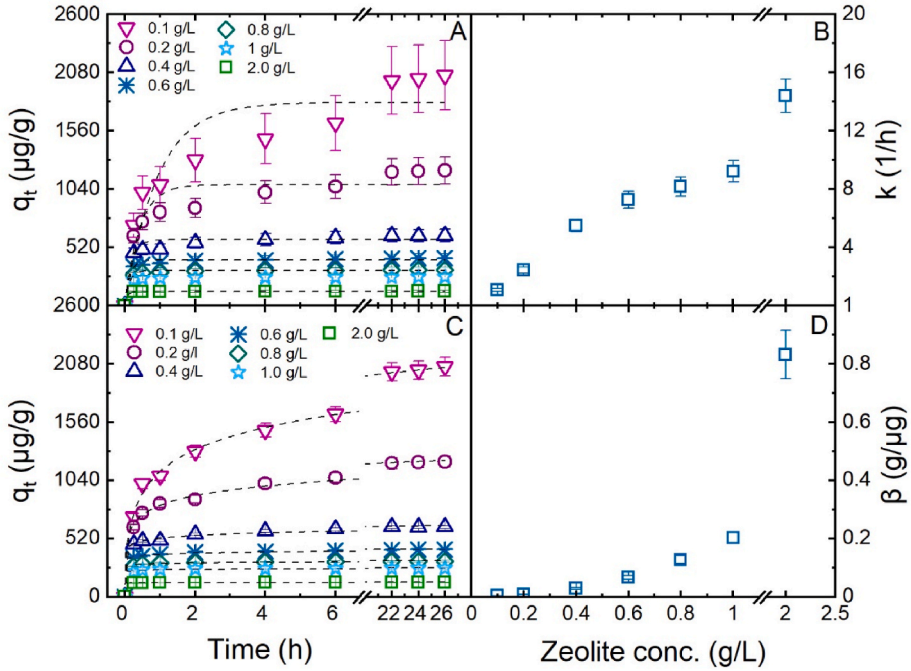

Fig. 5. Uranium adsorption kinetics for BEA-Fe30. Uranium uptake (q_t) as a function of time for (A) Pseudo-first order and (B) corresponding rate constant, (C) Elovich model, and (D) Elovich constant β for different zeolite concentrations. Initial uranium concentration: 250 µg/L, pH: 8.0 ± 0.1, 1 mM $NaHCO_3$, 10 mM NaCl, 20 °C, 260 rpm.

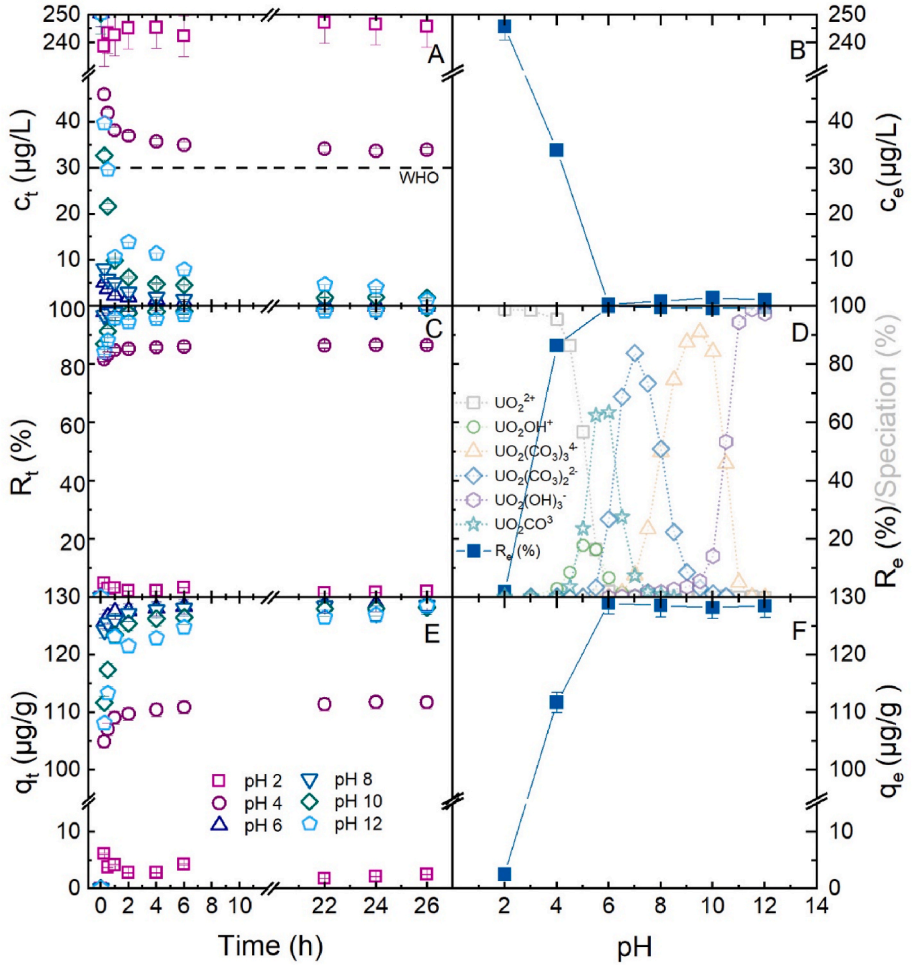

Fig. 6. (A) Uranium concentration in adsorbate solution; (C) Uranium removal; (E) Uranium uptake for BEA-Fe30 at pH 2–12 as a function of time. The corresponding values at equilibrium time (26 h) are shown on the right side (B, D, and F). Initial uranium concentration: 250 µg/L, 1 mM $NaHCO_3$, 10 mM NaCl, 20 °C, 260 rpm and 2g/L zeolite concentration. The open symbols in D presents the pH dependent speciation of uranium obtained by PHREEQC simulation.

uranium uptake observed at pH 6–12 is likely due to the formation of a U (VI)-carbonate ternary complex, as previously suggested by Davis and Randall (2001) and confirmed by Ulrich et al. (2006). In this mechanism, U(VI) binds directly to Fe oxide (hydr)oxo sites, with the carbonate ligands extending away from the oxide surface, facilitating increased uranium binding (Fig. 7).

In addition to the ternary complexes formed between Fe and U, uranyl ions may form $FeOUO_2^+$ which is one of the major complexes according to PHREEQC simulation. It is worth noting that the current PHREEQC model omits cation exchange at active sites, which may be critical for accurately characterizing low pH conditions. Low pH environments are not well represented by surface complexation alone, making cation exchange an important factor to consider.

Higher ionic strength is expected to reduce repulsive forces and

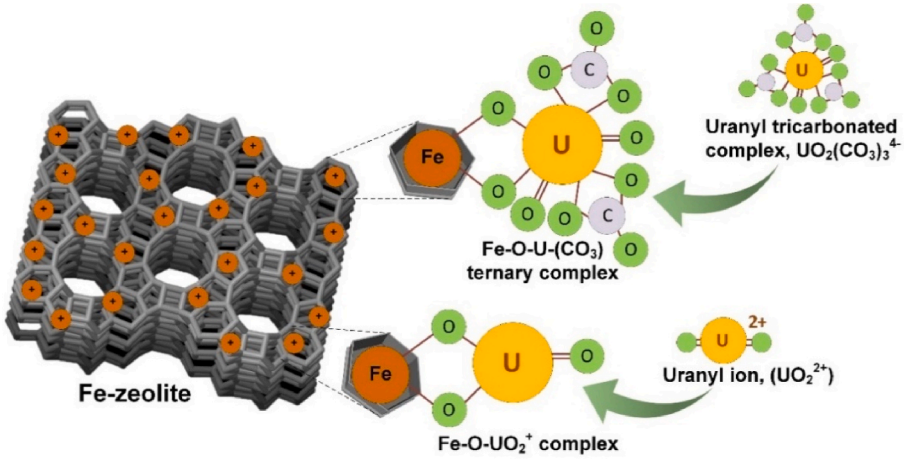

Fig. 7. Schematic representation of major iron-uranium complexes formed by UO_2^{2+} at acidic pHs and $UO_2(CO_3)_3^{4-}$ at alkaline pHs at the interface of Fe-zeolite.

enhance adsorption through electrostatic shielding and compression of the electrical double layer, while also affecting the chemical forms of uranium present in the solution. In consequence, the role of ionic strength in influencing uranium-zeolite interactions is further investigated.

3.5. Charge screening by ionic strength in uranium adsorption

The uranium uptake on zeolite could be due to interactions with the Fe on the surface by forming complexes (Ching-kuo Daniel and Langmuir, 1985; Davis and Randall, 2001), ion exchange interactions with the charged sites in the zeolite framework, or a combination of both. Ionic interaction of uranium can be suppressed by ionic strength. To differentiate mechanisms, adsorption experiments were performed at NaCl concentrations of 0.6–20.0 g/L. A reduction of uranium uptake with ionic strength would confirm charge interactions (Fig. 8).

Uranium uptake appears marginally higher at higher NaCl concentrations, with the difference between the experimental results and the theoretical model at different ionic strengths being more pronounced during the early stages of the experiment (0–6 h). While higher ionic strength typically reduces uranium adsorption due to ion competition, particularly at low pH (Nekhunguni et al., 2017; Khan et al., 2021), no such reduction was observed at elevated NaCl concentrations, at pH 8 (Fig. 8). During experimental conditions at equilibrium, there is no significant increase in uranium uptake beyond a critical salt concentration of 2.5 g/L, suggesting minimal competitive adsorption between uranium-carbonate complexes and salt ions under these conditions. The strong uranium uptake at ionic strengths below 2.5 g/L may be attributed to enhanced inner-sphere complexation, which facilitates the transport of uranium ions to the zeolite surface (Hayes and Leckie, 1987; Khan et al., 2021; Gandhi et al., 2022). At ionic strengths of 2.5 g/L or greater, the model and experimental data align, suggesting that despite changes in the electrical double layer thickness, the number of available surface sites and uranium-carbonate species remain constant in the system, resulting in no significant effect on uranium adsorption.

PHREEQC simulation at pH 8 (Fig. 8) does not reflect the variation in uranium uptake and removal observed in the experiment as the ionic strength increased from 0.6 to 2.5 g/L NaCl. In contrast, at an acidic pH of 2, the PHREEQC simulation (Fig. S15) shows that uranium removal and uptake increased from 5% to 22% as salinity increased from 0.1 to 20 g/L, likely due to the formation of chlorocomplexes such as UO_2Cl^+. The high uranium uptake at pH 8 and ionic strengths of 2.5 g/L or greater, observed in both the experiment and PHREEQC simulation, suggest that charge shielding by salt ions is less significant than inner-sphere surface complexation (Hayes and Leckie, 1987).

Static adsorption studies reveal the fundamental mechanisms and optimal conditions for uranium uptake, while filtration tests with zeolite-loaded membranes assess performance, including the effects of flow rates and zeolite loading. Such a thorough comparison will help optimizing uranium removal processes for practical applications.

3.6. Uranium removal by zeolite-loaded MF/UF with variable loading

Uranium filtration through zeolite-loaded MF/UF membranes

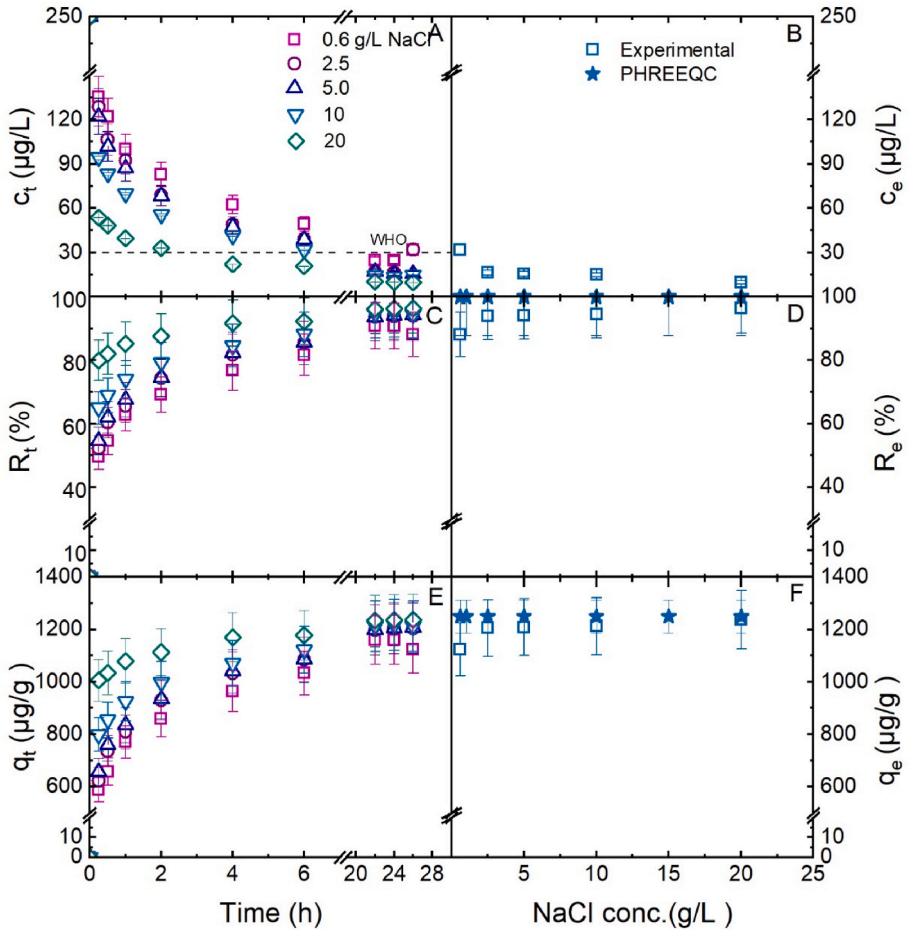

Fig. 8. (A) Uranium concentration in adsorbate solution; (C) Uranium removal; (E) uptake for BEA-Fe30 at NaCl concentrations (0.6–20.0 g/L). The corresponding values at equilibrium time (26 h), and PHREEQC simulation values are shown on the right side (B, D, and F). Initial uranium concentration: 250 µg/L, pH: 8.0 ± 0.1, 1 mM $NaHCO_3$, 20 °C, 260 rpm.

enhances mass transfer compared to static adsorption due to the reduction of boundary layers in the membrane pores. When pollutant concentrations are low, such boundary layers limit diffusion and hence adsorption kinetics. A uniform distribution of zeolite within the membrane is crucial to maximize surface area contact and facilitate efficient mass transfer. To verify the distribution of zeolite nanoparticles across the surface and within the pores of the MF membrane, SEM imaging was performed. The morphology of pristine zeolite nanoparticles and the zeolite-loaded composite membrane were analyzed as presented in Fig. 9.

SEM imaging reveals that zeolite BEA exhibits a well-defined spherical shape and a larger pore size, which enhance its adsorption capacity compared to zeolite Y (Figure S 14). The top-view SEM image of the zeolite-loaded composite membrane (Fig. 9D) confirms the distribution of zeolite particles on the surface and within the pores of the MF membrane.

The filtration at different zeolite loadings was performed to identify the minimum zeolite loading required for complete uranium removal (Fig. 10). Uranium permeate concentration and uptake on the zeolite increase with permeate volume. Zeolite loading resulted in a decreasing permeate uranium concentration, while removal improved. Uranium uptake approaches equilibrium at permeate volume 800 mL for a zeolite loading of 0.7 mg/cm^2 indicating that the adsorption sites become saturated, reaching a maximum capacity. This suggests that most of the available adsorption sites are occupied, and no further adsorption can occur at low zeolite loading. Uranium uptake increases linearly with the permeate volume for zeolite loadings greater than 1.3 mg/cm^2, suggesting that adsorption sites remain available and unsaturated throughout the process. Uranium uptake at the permeate volume 800 mL reduced by 66%, from 2080 to 699 μg/g, when the zeolite loading was increased by 89%, from 0.7 to 6.5 mg/cm^2.

While zeolite agglomeration, attributed to van der Waals forces, was evident at higher zeolite loadings (Fig. S12), no corresponding reduction in uranium uptake due to agglomeration was observed (Fig. 10). Although previous reports indicate that high concentration and surface energy can lead to significant agglomeration on the membrane, resulting in larger particles, potentially poor zeolite dispersion, and limited active surface area (Mahdavi Far et al., 2022), its effects on uranium uptake are not evident in this case. The incorporation of zeolite into the membrane's porous structure and surface appears to have mitigated agglomeration, ensuring better dispersion and accessibility. Therefore, the severity of agglomeration may be less pronounced here, contributing to minimal impact on uranium uptake compared to what is typically observed with zeolite in solution.

Membrane filtration with the MF/UF composite and static adsorption conditions cannot be directly compared for uranium removal. This is because static adsorption represents equilibrium conditions with longer hydraulic residence times and freely dispersed particles, while filtration involves forced flow, inevitably much shorter hydraulic residence times, and potentially reduced surface area due to zeolite loaded

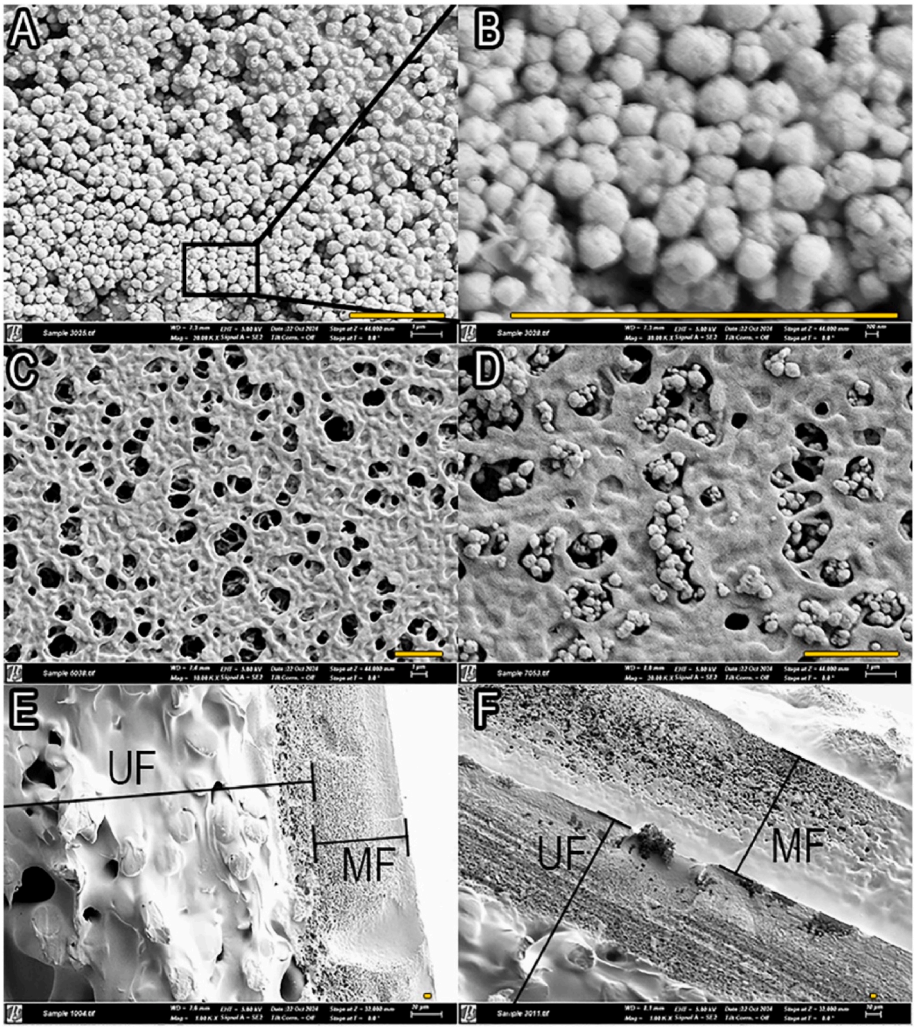

Fig. 9. SEM images of (A), (B) pristine zeolite BEA-Fe30; (C), (E) pristine MF (cellulose nitrate, 0.45 μm) and (D), (F) 6.5 mg/cm^2 zeolite BEA-Fe30 loaded MF/UF (PMBK 300 kDa) stacked membrane. (C) and (D) are top-view; (E) and (F) are cross-section view. Scale bars inside all images represent 3 μm.

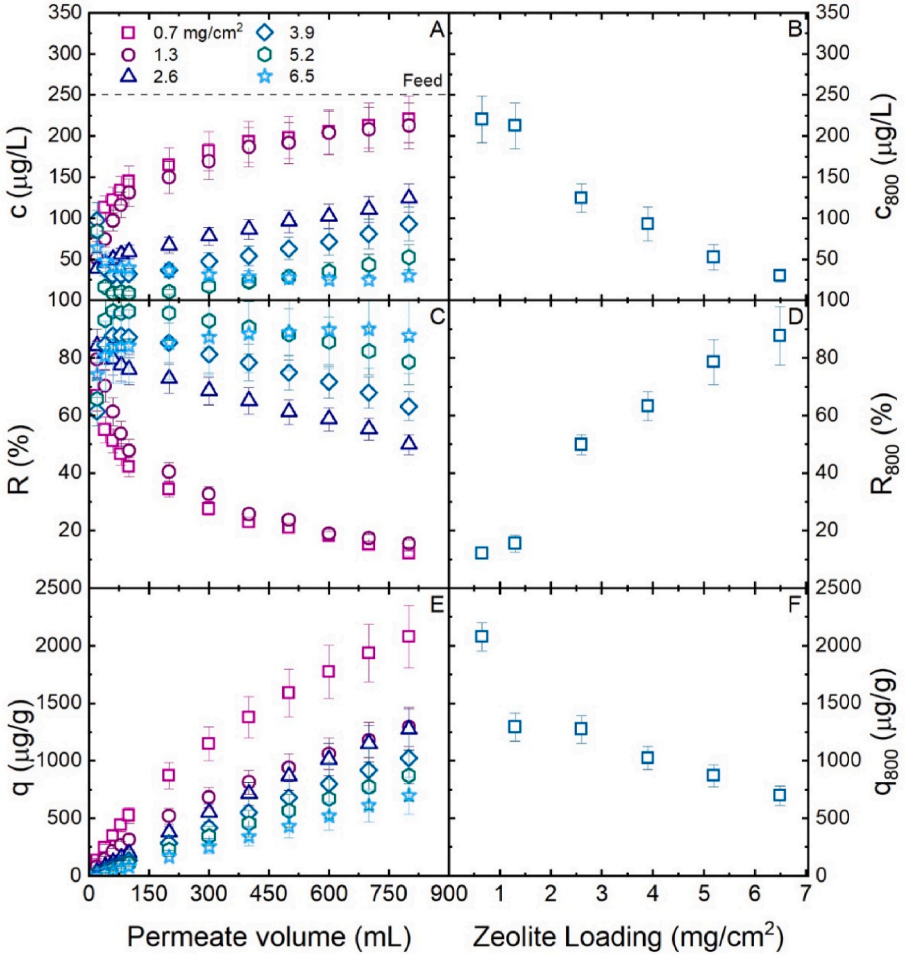

Fig. 10. (A) Uranium concentration in permeate; (C) Uranium removal; and (E) Uranium uptake as a function of permeate volume for different zeolite loadings. The corresponding values at the end of filtration (at 800 mL permeate) are shown on the right side (B, D, and F) as a function of zeolite loading (B) U (VI) uptake as a function of zeolite loading. MF (cellulose nitrate, 0.45 µm)/UF (PMBK 300 kDa) stacked membranes. Initial uranium concentration: 250 µg/L, 1 mM $NaHCO_3$, 10 mM NaCl, 20 ± 0.1 °C, pH: 8.0 ± 0.1, flow rate: 1.0 L/h.

in membranes. Mass transfer limitations affect both methods differently, with static adsorption facing slower diffusion limited rates, where contact in membrane filtration is determined by flow rate and membrane properties. Uranium adsorption is presented as a function of zeolite loading in Fig. S9 in order to give a basic comparative understanding of uranium removal under static adsorption (at 26 h of contact time) and membrane filtration conditions (at permeate volume 800 mL and 1 L/h flow rate, equivalent to 0.8 h of contact time).

At very low zeolite mass ≤0.05 g, both static adsorption and MF/UF filtration show comparable uranium uptake. As zeolite mass increases beyond 0.1 g, the disparity between the two methods becomes more pronounced. At a zeolite mass of 0.25 g, static adsorption results in a uranium uptake of 256 µg/g of zeolite, whereas MF/UF results in a significantly higher uptake of 699 µg/g. This indicates that mass transfer limitations can be overcome by immobilizing the zeolites in a membrane.

Increasing the hydraulic residence time in zeolize-loaded MF/UF filtration condition is expected to further enhance uranium uptake. Contributing factors are more time for adsorption interactions, improving diffusion to internal sites, reducing flow rates, ensuring fuller saturation of the adsorbent, delayed breakthrough, and approaching equilibrium conditions.

3.7. Uranium removal by zeolite-loaded MF/UF with variable hydraulic residence time

Different flow rates were applied to analyze the variation in uranium uptake with hydraulic residence time (Fig. 11).

As expected, lower hydraulic residence time at increased flow rate results in higher uranium concentrations in the permeate and lower uranium removal. The uranium uptake is reduced by the flow rate, at a permeate volume of 800 mL uptake is reduced by 33%, from 1178 to 786 µg/g as the flow rate increased by 80%, from 0.2 to 1.0 L/h. The decrease in uranium uptake with flow rate suggests that the hydraulic residence time affects removal. It appears that uranium removal during MF/UF filtration is limited by mass transfer processes such as micropore diffusion (Mahdavi Far et al., 2022) and adsorption onto the zeolite. The sorption kinetics of the uranium onto zeolite are relatively fast, allowing for effective removal at a low (0.1 L/h) to moderate (0.6 L/h) flow rates. However, at higher flow rates, the diffusion of uranium ions from the bulk solution to the surface of the zeolite particles becomes less effective and ultimately limiting. In other words, the ions lack the time to diffuse into the pores of the zeolite, where most adsorption sites are located. While an increasing flow rate can lead to a thinner boundary layer around the zeolite particles, such a boundary layer is minimal in a membrane pore and not limiting.

Uranium filtration through zeolite-loaded MF/UF membranes reveals better mass transfer compared to static adsorption, while adequate

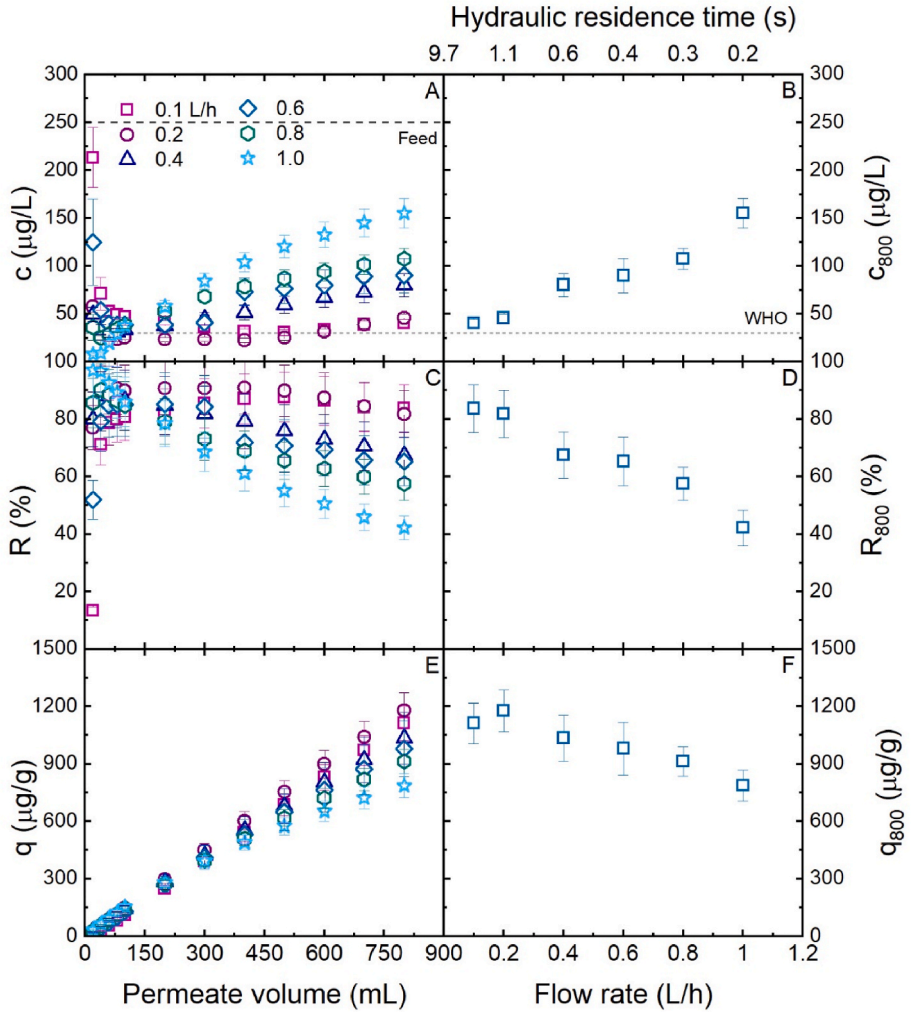

Fig. 11. (A) Uranium concentration in permeate; (C) Uranium removal; and (E) Uranium uptake as a function of permeate volume for different flow rates. The corresponding values at the end of filtration (at 800 mL permeate) are shown on the right side (B, D, and F) as a function of flow rates. MF (cellulose nitrate, 0.45 µm)/UF (PMBK 300 kDa) stacked membranes Initial uranium concentration: 250 µg/L, 1 mM $NaHCO_3$, 10 mM NaCl, 20 ± 0.1 °C, pH: 8.0 ± 0.1.

hydraulic residence time is critical to enhance adsorption. The hydraulic residence time of 0.2–10 s used in this work is 1–2 orders of magnitude lower than the hydraulic residence times typically used in nanofiltration (Imbrogno and Schäfer, 2021). Increasing the zeolite loading decreases uranium concentration in the permeate, enhancing removal, while uptake remains stable. Higher flow rates decrease removal efficiency due to the reduced hydraulic residence and thus contact time, suggesting mass transfer limitations.

4. Conclusions

This study highlights the potential of zeolites and zeolite composite membranes, specifically iron-modified zeolites, for efficient uranium removal from water. Both static adsorption and membrane filtration were employed, focusing on the effects of zeolite loading, hydraulic residence time, and mass transfer in zeolite-MF/UF composite membranes. Initial tests on different zeolites showed that those with high Si/Al ratios exhibited the highest uranium adsorption capacity. PHREEQC simulations confirmed that uranium removal increased with higher Si/Al ratios, particularly in neutral to alkaline pH conditions.

Detailed studies using Fe-incorporated zeolite BEA-Fe30 demonstrated complete uranium removal at a zeolite loading of 0.6 g/L, with uranium uptake ranging from 125 to 130 µg/g at pH 6–12, decreasing to 111 µg/g at pH 4 and 3 µg/g at pH 2. The formation of U(VI)-carbonate ternary complex, where U(VI) binds to Fe oxide surface (hydr)oxo sites, likely contributes to the higher uranium adsorption at neutral to alkaline pH. Increased ionic strength (0.6–2.5 g/L NaCl) enhanced uranium adsorption, as observed in static adsorption experiments. However, a further increase in ionic strength at pH 8 showed no additional effect, as confirmed by PHREEQC modeling, indicating that inner-sphere surface complexation is likely the dominant mechanism at alkaline pH. Filtration through zeolite-loaded MF/UF membranes resulted in faster and more effective uranium removal by reducing boundary layer limitations. At a zeolite mass above 0.1 g, the difference between static adsorption and membrane filtration became evident, with static adsorption achieving a uranium uptake of 256 µg/g and MF/UF reaching 699 µg/g at 0.25 g zeolite. MF/UF membrane uranium adsorption was flow rate-dependent, indicating that uranium removal during filtration may be limited by mass transfer processes such as micropore diffusion and adsorption onto the zeolite.

Zeolite composite membranes offer a promising, scalable solution for uranium and heavy metal removal from water. Further research on membrane stability, selective adsorption, and regeneration techniques by desorption is essential to fully optimize their potential. Adopting a circular economy approach, the regeneration and reusability of the zeolite composite membranes will enhance sustainability by minimizing waste and recovering valuable uranium for reuse. The use of diverse zeolites and adsorbents presents significant potential for developing

sustainable composite materials, particularly in regions where local materials can be utilized, supporting both environmental and economic sustainability.

CRediT authorship contribution statement

Akhil Gopalakrishnan: Writing – original draft, Supervision, Methodology, Investigation, Formal analysis, Data curation, Conceptualization. **Stephen Asare:** Investigation, Data curation. **Francis Adu-Boahene:** Writing – review & editing, Methodology, Investigation, Formal analysis, Data curation. **Andrea I. Schäfer:** Writing – review & editing, Supervision, Resources, Project administration, Methodology, Funding acquisition, Conceptualization.

Declaration of competing interest

The authors declare that they have no known competing financial interests or personal relationships that could have appeared to influence the work reported in this paper.

Acknowledgements

The Helmholtz Association provided funding for the research at IAMT through the Recruitment Initiative, and the Deutsche Forschungsgemeinschaft (DFG) is thanked for funding under the scheme DFG-Kooperation mit Subsahara-Afrika 2020: IIC - Solar Energy. Prof. Francis WY Momade, Kwame Nkrumah University of Science and Technology (KNUST), Ghana, for his contributions to the funding application, his short research stay and for discussions on zeolite properties with Prof. Dr. Bryce S. Richards, Institute of Microstructure Technology (IMT), Karlsruhe Institute of Technology (KIT); Dr. Richard Opoku and Dr. David Ato Quansah, Kwame Nkrumah University of Science and Technology (KNUST), Ghana, as collaborators for the DFG funding application. The Katholischer Akademischer Ausländer Dienst (KAAD) is thanked for providing a Ph.D. scholarship to Francis Adu-Boahene, Dr. Gabriel Tkacik Millipore (Bedford) is acknowledged for the provision of UF membranes and Dr.-Ing. Jens Freiding and Dr. Silke Sauerbeck, Clariant Produkte (Deutschland) GmbH, Germany for the zeolite samples. Dr. Youssef-Amine Boussouga (IAMT) for ICP-MS analysis and managing the purchase and health and safety of uranium at IAMT; the Office of Safety and Environment (SUM) at KIT for facilitating technical regulation and health and safety measures for working with uranium; Dr. Justine Nyarige (IMT) provided the SEM imaging and XRD analysis; Dr. Andrey Turshatov (IMT) enabled access to the DLS instrument; Dr. Minh Nguyen (IAMT) carried out DLS measurements and discussed the manuscript; while Dr. Teba Gil-Díaz (Institute of Applied Geosciences, KIT) reviewed the PHREEQC modelling.

Appendix A. Supplementary data

Supplementary data to this article can be found online at https://doi.org/10.1016/j.chemosphere.2024.143711.

Data availability

Data will be made available on request.

References

Abdi, M.R., Shakur, H.R., Rezaee Ebrahim Saraee, K., Sadeghi, M., 2014. Effective removal of uranium ions from drinking water using CuO/X zeolite based nanocomposites: effects of nano concentration and cation exchange. J. Radioanal. Nucl. Chem. 300, 1217–1225.

Abolli, S., Borhani Yazdi, N., Khanizadeh, M., Salemi, K., Bidoki, M.Z., Mehrizi, E.A., 2024. Understanding uranium distribution: a systematic review and meta-analysis in the context of drinking water resources. Results Eng 22, 102152.

Aghadavoud, A., Saraee, K.R.E., Shakur, H.R., Sayyari, R., 2016. Removal of uranium ions from synthetic wastewater using ZnO/Na-clinoptilolite nanocomposites. Radiochim. Acta 104, 809–819.

Aharoni, C., Tompkins, F.C., 1970. Kinetics of adsorption and desorption and the Elovich equation. In: Eley, D.D., Pines, H., Weisz, P.B. (Eds.), Advances in Catalysis. Academic Press, pp. 1–49.

Akash, S., Sivaprakash, B., Raja, V.C.V., Rajamohan, N., Muthusamy, G., 2022. Remediation techniques for uranium removal from polluted environment – review on methods, mechanism and toxicology. Environ. Pollut. 302, 119068.

Arnold, T., Zorn, T., Zänker, H., Bernhard, G., Nitsche, H., 2001. Sorption behavior of U (VI) on phyllite: experiments and modeling. J. Contam. Hydrol. 47, 219–231.

Aytas, S.O., Akyil, S., Eral, M., 2004. Adsorption and thermodynamic behavior of uranium on natural zeolite. J. Radioanal. Nucl. Chem. 260, 119–125.

Bachmaf, S., Merkel, B.J., 2011. Sorption of uranium(VI) at the clay mineral–water interface. Environ. Earth Sci. 63, 925–934.

Baerlocher, C., McCusker, L.B., Olson, D.H., 2007. Atlas of Zeolite Framework Types, Sixth Revised Edition ed. Elsevier, The Netherlands.

Barkat, M., Nibou, D., Amokrane, S., Chegrouche, S., Mellah, A., 2015. Uranium (VI) adsorption on synthesized 4A and P1 zeolites: equilibrium, kinetic, and thermodynamic studies. Compt. Rendus Chem. 18, 261–269.

Bayramoglu, G., Arica, M.Y., 2016. MCM-41 silica particles grafted with polyacrylonitrile: modification in to amidoxime and carboxyl groups for enhanced uranium removal from aqueous medium. Microporous Mesoporous Mater. 226, 117–124.

Boussouga, Y.-A., Joseph, J., Stryhanyuk, H., Richnow, H.H., Schäfer, A.I., 2024. Adsorption of uranium (VI) complexes with polymer-based spherical activated carbon. Water Res. 249, 120825.

Boussouga, Y.-A., Tantish, F., Schäfer, A.I., 2022. MF/UF Hematite Loaded Composite Membranes for Arsenate and Arsenite Removal (unpublished work).

Boussouga, Y.-A., Tantish, F., Schäfer, A.I., 2023. Microporous hematite-loaded composite membrane for arsenic(III) and arsenic(V) removal. ACS Appl. Eng. Mater. 1, 1164–1175.

Bundesgesetzblatt, 2023. Zweite Verordnung zur Novellierung der Trinkwasserverordnung. Bonn, Germany.

Camacho, L.M., Deng, S., Parra, R.R., 2010. Uranium removal from groundwater by natural clinoptilolite zeolite: effects of pH and initial feed concentration. J. Hazard Mater. 175, 393–398.

Chien, S., Clayton, W., 1980. Application of Elovich equation to the kinetics of phosphate release and sorption in soils. Soil Sci. Soc. Am. J. 44, 265–268.

Ching-kuo Daniel, H., Langmuir, D., 1985. Adsorption of uranyl onto ferric oxyhydroxides: application of the surface complexation site-binding model. Geochem. Cosmochim. Acta 49, 1931–1941.

Choppin, G.R., Jensen, M.P., 2006. Actinides in solution: complexation and kinetics. In: Morss, L.R., Edelstein, N.M., Fuger, J. (Eds.), The Chemistry of the Actinide and Transactinide Elements. Springer, Netherlands, Dordrecht, pp. 2524–2621.

Coutelot, F.M., Seaman, J.C., Baker, M., 2018. Uranium(VI) adsorption and surface complexation modeling onto vadose sediments from the Savannah River Site. Environ. Earth Sci. 77, 148.

Damiania, L.H., Marcos Antonio, K., Mara, A., Carla Dal Sasso, F., Anthony, J.P., 2015. SHPECK-A Geochemical Speciation Modeling Software. Universidade Federal Do Rio Grande Do Sul.

Davis, J.A., Randall, J.D., 2001. Surface Complexation Modeling of Uranium (VI) Adsorption on Natural Mineral Assemblages. U.S. Geological Survey, Washington, DC, pp. 1–214.

Davoodbeygi, Y., Askari, M., Salehi, E., Kheirieh, S., 2023. A review on hybrid membrane-adsorption systems for intensified water and wastewater treatment: process configurations, separation targets, and materials applied. J. Environ. Manag. 335, 117577.

Dzombak, D.A., Morel, F.M., 1990. Surface Complexation Modeling: Hydrous Ferric Oxide. John Wiley & Sons, New York.

Ektefa, F., Towfighi Darian, J., Soltanali, S., 2022. Performance of BEA, FAU, LTL, MFI, and MOR zeolites in the removal of ethyl mercaptan traces from natural gas by Monte Carlo molecular simulation. Appl. Surf. Sci. 605, 154833.

Fatima, H., Djamel, N., Samira, A., Mahfoud, B., 2013. Modelling and adsorption studies of removal uranium (VI) ions on synthesised zeolite NaY. Desalination Water Treat. 51, 5583–5591.

Gandhi, T.P., Sampath, P.V., Maliyekkal, S.M., 2022. A critical review of uranium contamination in groundwater: treatment and sludge disposal. Sci. Total Environ. 825, 153947.

Graça, I., Bacariza, M.C., Fernandes, A., Chadwick, D., 2018. Desilicated NaY zeolites impregnated with magnesium as catalysts for glucose isomerisation into fructose. Appl. Catal., B 224, 660–670.

Grenthe, I., Fuger, J., Konings, R.J.M., Lemire, R.J., Muller, A.B., Nguyen-Trung Cregu, C., Wanner, H., 1992. Chemical Thermodynamics of Uranium. Elsevier Science Ltd, Amsterdam.

Guimarães, V., Rodríguez-Castellón, E., Algarra, M., Rocha, F., Bobos, I., 2016. Influence of pH, layer charge location and crystal thickness distribution on U(VI) sorption onto heterogeneous dioctahedral smectite. J. Hazard Mater. 317, 246–258.

Guo, Z., Yan, C., Xu, J., Wu, W., 2009. Sorption of U(VI) and phosphate on γ-alumina: binary and ternary sorption systems. Colloids Surf., A 336, 123–129.

Han, R., Zou, L., Zhao, X., Xu, Y., Xu, F., Li, Y., Wang, Y., 2009. Characterization and properties of iron oxide-coated zeolite as adsorbent for removal of copper(II) from solution in fixed bed column. Chem. Eng. J. 149, 123–131.

Haneklaus, S.H., Windmann, H., Maekawa, M., Zhang, L., Schnug, E., 2021. Diet controls uranium intake and aggravates health hazards. Med. Res. Arch. 9.

Hao, S., Jia, Z., Wen, J., Li, S., Peng, W., Huang, R., Xu, X., 2021. Progress in adsorptive membranes for separation – a review. Sep. Purif. Technol. 255, 117772.
Hayes, K.F., Leckie, J.O., 1987. Modeling ionic strength effects on cation adsorption at hydrous oxide/solution interfaces. J. Colloid Interface Sci. 115, 564–572.
He, T., Li, Q., Lin, T., Li, J., Bai, S., An, S., Kong, X., Song, Y.-F., 2023. Recent progress on highly efficient removal of heavy metals by layered double hydroxides. Chem. Eng. J. 462, 142041.
Health Canada, 2019. Guidelines for Canadian Drinking Water Quality Guideline Technical Document - Uranium. Ottawa.
Ighalo, J.O., Chen, Z., Ohoro, C.R., Oniye, M., Igwegbe, C.A., Elimhingbovo, I., Khongthaw, B., Dulta, K., Yap, P.-S., Anastopoulos, I., 2024. A review of remediation technologies for uranium-contaminated water. Chemosphere 352, 141322.
Imbrogno, A., Nguyen, M.N., Schäfer, A.I., 2024. Tutorial review of error evaluation in experimental water research at the example of membrane filtration. Chemosphere 357, 141833.
Imbrogno, A., Schäfer, A.I., 2019. Comparative study of nanofiltration membrane characterization devices of different dimension and configuration (cross flow and dead end). J. Membr. Sci. 585, 67–80.
Imbrogno, A., Schäfer, A.I., 2021. Micropollutants breakthrough curve phenomena in nanofiltration: impact of operational parameters. Sep. Purif. Technol. 267, 118406.
Iwasaki, M., Yamazaki, K., Banno, K., Shinjoh, H., 2008. Characterization of Fe/ZSM-5 DeNOx catalysts prepared by different methods: relationships between active Fe sites and NH3-SCR performance. J. Catal. 260, 205–216.
Jiménez-Reyes, M., Almazán-Sánchez, P.T., Solache-Ríos, M., 2021. Radioactive waste treatments by using zeolites. A short review. J. Environ. Radioact. 233, 106610.
Jun, B.-M., Lee, H.-K., Park, S., Kim, T.-J., 2021. Purification of uranium-contaminated radioactive water by adsorption: a review on adsorbent materials. Sep. Purif. Technol. 278, 119675.
Kalintsev, A., Guan, Q., Brugger, J., Migdisov, A., Etschmann, B., Ram, R., Liu, W., Mei, Y., Testemale, D., Xu, H., 2023. Nature and coordination geometry of geologically relevant aqueous Uranium(VI) complexes up to 400 °C: a review and new data. J. Hazard Mater. 452, 131309.
Khan, S., Anjum, R., Bilal, M., 2021. Revealing chemical speciation behaviors in aqueous solutions for uranium (VI) and europium (III) adsorption on zeolite. Environ. Technol. Innov. 22, 101503.
Kilincarslan, A., Akyil, S., 2005. Uranium adsorption characteristic and thermodynamic behavior of clinoptilolite zeolite. J. Radioanal. Nucl. Chem. 264, 541–548.
Kong, L., Zhu, Y., Wang, M., Li, Z., Tan, Z., Xu, R., Tang, H., Chang, X., Xiong, Y., Chen, D., 2016. Simultaneous reduction and adsorption for immobilization of uranium from aqueous solution by nano-flake Fe-SC. J. Hazard Mater. 320, 435–441.
Korichi, S., Bensmaili, A., 2009. Sorption of uranium (VI) on homoionic sodium smectite experimental study and surface complexation modeling. J. Hazard Mater. 169, 780–793.
Król, M., Mozgawa, W., Jastrzębski, W., 2016. Theoretical and experimental study of ion-exchange process on zeolites from 5-1 structural group. J. Porous Mater. 23, 1–9.
Lagergren, S., 1898. About the theory of so-called adsorption of soluble substances. Kungliga Svenska Vetenskapsakademiens 24, 1–39.
Largitte, L., Pasquier, R., 2016. A review of the kinetics adsorption models and their application to the adsorption of lead by an activated carbon. Chem. Eng. Res. Des. 109, 495–504.
Li, C., Gao, X., Li, S., Bundschuh, J., 2020a. A review of the distribution, sources, genesis, and environmental concerns of salinity in groundwater. Environ. Sci. Pollut. Res. 27, 41157–41174.
Li, J., Gao, M., Yan, W., Yu, J., 2023. Regulation of the Si/Al ratios and Al distributions of zeolites and their impact on properties. Chem. Sci. 14, 1935–1959.
Li, X., Liu, Z., Huang, M., 2022a. Purification of uranium-containing wastewater by adsorption: a review of research on resin materials. J. Radioanal. Nucl. Chem. 331, 3043–3075.
Li, Y., Simon, A.O., Jiao, C., Zhang, M., Yan, W., Rao, H., Liu, J., Zhang, J., 2020b. Rapid removal of Sr2+, Cs+ and UO22+ from solution with surfactant and amino acid modified zeolite Y. Microporous Mesoporous Mater. 302, 110244.
Li, Z., Tang, D., Dai, Y., Zou, R., Liu, H., Tao, Q., Liu, Z., 2022b. Fabrication of a novel electrospun polyvinyl alcohol/polyacrylic acid nanofiber adsorbent loading with montmorillonite or zeolite for uranium (VI) removal. J. Radioanal. Nucl. Chem. 331, 297–307.
Lövgren, L., Sjöberg, S., Schindler, P.W., 1990. Acid/base reactions and Al(III) complexation at the surface of goethite. Geochem. Cosmochim. Acta 54, 1301–1306.
Luo, W., Kelly, S.D., Kemner, K.M., Watson, D., Zhou, J., Jardine, P.M., Gu, B., 2009. Sequestering uranium and technetium through Co-precipitation with aluminum in a contaminated acidic environment. Environ. Sci. Technol. 43, 7516–7522.
Mahdavi Far, R., Van der Bruggen, B., Verliefde, A., Cornelissen, E., 2022. A review of zeolite materials used in membranes for water purification: history, applications, challenges and future trends. J. Chem. Technol. Biotechnol. 97, 575–596.
Maher, K., Bargar, J.R., Brown, G.E., 2013. Environmental speciation of actinides. Inorg. Chem. 52, 3510–3532.
Mahoney, J.J., Cadle, S.A., Jakubowski, R.T., 2009. Uranyl adsorption onto hydrous ferric oxide—a re-evaluation for the diffuse layer model database. Environ. Sci. Technol. 43, 9260–9266.
Maier, S.M., Jentys, A., Janousch, M., van Bokhoven, J.A., Lercher, J.A., 2012. Unique dynamic changes of Fe cationic species under NH3-SCR conditions. J. Phys. Chem. C 116, 5846–5856.
Mangini, A., Sonntag, C., Bertsch, G., Müller, E., 1979. Evidence for a higher natural uranium content in world rivers. Nature 278, 337–339.
MHLW, 2015. Fundamental Principle of the Current Drinking Water Quality Standards. Ministry of Health, Labour and Welfare, Japan.
Mittal, H., Alfantazi, A.M., Alhassan, S.M., 2024. Recent developments in the adsorption of uranium ions from wastewater/seawater using carbon-based adsorbents. J. Environ. Chem. Eng. 12, 111705.
Mosai, A.K., Johnson, R.H., Tutu, H., 2021. Modelling of palladium(II) adsorption onto amine-functionalised zeolite using a generalised surface complexation approach. J. Environ. Manag. 277, 111416.
Nah, I.W., Hwang, K.-Y., Jeon, C., Choi, H.B., 2006. Removal of Pb ion from water by magnetically modified zeolite. Miner. Eng. 19, 1452–1455.
Nazir, L.S.M., Yeong, Y.F., Chew, T.L., 2020. Methods and synthesis parameters affecting the formation of FAU type zeolite membrane and its separation performance: a review. J. Asian Ceram. Soc. 8, 553–571.
Nekhunguni, P.M., Tavengwa, N.T., Tutu, H., 2017. Sorption of uranium(VI) onto hydrous ferric oxide-modified zeolite: assessment of the effect of pH, contact time, temperature, selected cations and anions on sorbent interactions. J. Environ. Manag. 204, 571–582.
Nibou, D., Khemaissia, S., Amokrane, S., Barkat, M., Chegrouche, S., Mellah, A., 2011. Removal of UO22+ onto synthetic NaA zeolite. Characterization, equilibrium and kinetic studies. Chem. Eng. J. 172, 296–305.
Olguín, M.T., Solache-Ríos, M., Acosta, D., Bosch, P., Bulbulian, S., 1999. Uranium sorption in zeolite X: the valence effect. Microporous Mesoporous Mater. 28, 377–385.
Östhols, E., 1995. Thorium sorption on amorphous silica. Geochem. Cosmochim. Acta 59, 1235–1249.
Parkhurst, D.L., Appelo, C.A.J., 2013. Description of input and examples for PHREEQC version 3—a computer program for speciation, batch-reaction, one-dimensional transport, and inverse geochemical calculations. US Geological Survey Techniques and Methods 6, 497.
Qasem, N.A.A., Mohammed, R.H., Lawal, D.U., 2021. Removal of heavy metal ions from wastewater: a comprehensive and critical review. npj Clean Water 4, 36.
Raff, O., Wilken, R.-D., 1999. Removal of dissolved uranium by nanofiltration. Desalination 122, 147–150.
Rani, L., Srivastav, A.L., Kaushal, J., Shukla, D.P., Pham, T.D., van Hullebusch, E.D., 2023. Significance of MOF adsorbents in uranium remediation from water. Environ. Res. 236, 116795.
Rudzinski, W., Plazinski, W., 2006. Kinetics of solute adsorption at solid/solution interfaces: a theoretical development of the empirical pseudo-first and pseudo-second order kinetic rate equations, based on applying the statistical rate theory of interfacial transport. J. Phys. Chem. B 110, 16514–16525.
Sahoo, T.R., Prelot, B., 2020. Chapter 7 - adsorption processes for the removal of contaminants from wastewater: the perspective role of nanomaterials and nanotechnology. In: Bonelli, B., Freyria, F.S., Rossetti, I., Sethi, R. (Eds.), Nanomaterials for the Detection and Removal of Wastewater Pollutants. Elsevier, pp. 161–222.
Sen Gupta, S., Bhattacharyya, K.G., 2011. Kinetics of adsorption of metal ions on inorganic materials: a review. Adv. Colloid Interface Sci. 162, 39–58.
Shen, J., Schäfer, A., 2014. Removal of fluoride and uranium by nanofiltration and reverse osmosis: a review. Chemosphere 117, 679–691.
Silva, R.J., Nitsche, H., 1995. Actinide environmental chemistry. Radiochim. Acta 70–71, 377–396.
Smedley, P.L., Kinniburgh, D.G., 2023. Uranium in natural waters and the environment: distribution, speciation and impact. Appl. Geochem. 148, 105534.
Su, H., Kim, H.S., Seo, S.M., Ko, S.O., Suh, J.M., Kim, G.H., Lim, W.T., 2012. Location of Na^+ ions in fully dehydrated Na^+ saturated zeolite Y (FAU, Si/Al = 1.56). Bull. Kor. Chem. Soc. 33, 2785–2788.
Tarach, K.A., Tekla, J., Filek, U., Szymocha, A., Tarach, I., Góra-Marek, K., 2017. Alkaline-acid treated zeolite L as catalyst in ethanol dehydration process. Microporous Mesoporous Mater. 241, 132–144.
Turner, G.D., Zachara, J.M., McKinley, J.P., Smith, S.C., 1996. Surface-charge properties and UO22+ adsorption of a subsurface smectite. Geochem. Cosmochim. Acta 60, 3399–3414.
Uddin, M.K., 2017. A review on the adsorption of heavy metals by clay minerals, with special focus on the past decade. Chem. Eng. J. 308, 438–462.
Ulrich, K.-U., Rossberg, A., Foerstendorf, H., Zänker, H., Scheinost, A.C., 2006. Molecular characterization of uranium(VI) sorption complexes on iron(III)-rich acid mine water colloids. Geochem. Cosmochim. Acta 70, 5469–5487.
USGS, 2021. PHREEQC Version 3.
Vasconcelos, A.A., Len, T., de Oliveira, A.d.N., Costa, A.A.F.d., Souza, A.R.d.S., Costa, C. E.F.d., Luque, R., Rocha Filho, G.N.d., Noronha, R.C.R., Nascimento, L.A.S.d., 2023. Zeolites: a theoretical and practical approach with uses in (bio)chemical processes. Appl. Sci. 13, 1897.
Waite, T.D., Davis, J.A., Payne, T., Waychunas, G.A., Xu, N., 1994. Uranium(VI) adsorption to ferrihydrite: application of a surface complexation model. Geochem. Cosmochim. Acta 58, 5465–5478.
Wang, L., Song, H., Yuan, L., Li, Z., Zhang, Y., Gibson, J.K., Zheng, L., Chai, Z., Shi, W., 2018. Efficient U(VI) reduction and sequestration by Ti2CTx MXene. Environ. Sci. Technol. 52, 10748–10756.
Wang, Y., Liu, X., Xie, Y., Chen, B., Zhang, Y., 2022. Effective and rapid adsorption of uranium via synergy of complexation and cation-π interaction. J. Radioanal. Nucl. Chem. 331, 1115–1126.
Wazne, M., Korfiatis, G.P., Meng, X., 2003. Carbonate effects on hexavalent uranium adsorption by iron oxyhydroxide. Environ. Sci. Technol. 37 (16), 3619–3624.
WHO, 2017. Guidelines for drinking-water quality. Fourth Edition Incorporating the First Addendum. World Health Organization, Geneva.
Xie, Y., Chen, C., Ren, X., Wang, X., Wang, H., Wang, X., 2019. Emerging natural and tailored materials for uranium-contaminated water treatment and environmental remediation. Prog. Mater. Sci. 103, 180–234.

Xing, C., Bernicot, B., Arrachart, G., Pellet-Rostaing, S., 2023. Application of ultra/nano filtration membrane in uranium rejection from fresh and salt waters. Sep. Purif. Technol. 314, 123543.
Yue, B., Liu, S., Chai, Y., Wu, G., Guan, N., Li, L., 2022. Zeolites for separation: fundamental and application. J. Energy Chem. 71, 288–303.
Zachara, J.M., McKinley, J.P., 1993. Influence of hydrolysis on the sorption of metal cations by smectites: importance of edge coordination reactions. Aquat. Sci. 55, 250–261.
Zhang, Q., Gao, S., Yu, J., 2023. Metal sites in zeolites: synthesis, characterization, and catalysis. Chem. Rev. 123, 6039–6106.
Zong, P., Wang, H., Pan, H., Zhao, Y., He, C., 2013a. Application of NKF-6 zeolite for the removal of U(VI) from aqueous solution. J. Radioanal. Nucl. Chem. 295, 1969–1979.
Zong, P., Wang, S., Zhao, Y., Wang, H., Pan, H., He, C., 2013b. Synthesis and application of magnetic graphene/iron oxides composite for the removal of U(VI) from aqueous solutions. Chem. Eng. J. 220, 45–52.
Zou, W., Bai, H., Zhao, L., Li, K., Han, R., 2011. Characterization and properties of zeolite as adsorbent for removal of uranium(VI) from solution in fixed bed column. J. Radioanal. Nucl. Chem. 288, 779–788.
Zou, W., Zhao, L., Han, R., 2009. Removal of uranium (VI) by fixed bed ion-exchange column using natural zeolite coated with manganese oxide. Chin. J. Chem. Eng. 17, 585–593.
Zou, Y., Liu, Y., Wang, X., Sheng, G., Wang, S., Ai, Y., Ji, Y., Liu, Y., Hayat, T., Wang, X., 2017. Glycerol-modified binary layered double hydroxide nanocomposites for uranium immobilization via extended X-ray absorption fine structure technique and density functional theory calculation. ACS Sustainable Chem. Eng. 5, 3583–3595.